Journal Pre-proof

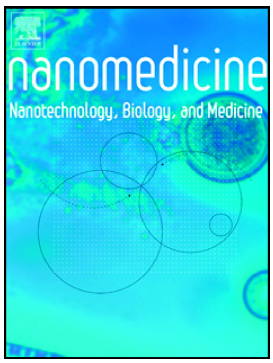

Nanostructured scaffolds based on Bioresorbable polymers and Graphene oxide induce the aligned migration and accelerate the neuronal differentiation of neural stem cells

Y. Polo, J. Luzuriaga, J. Iturri, I. Irastorza, J.L. Toca-Herrera, G. Ibarretxe, F. Unda, J.R. Sarasua, J.R. Pineda, A. Larrañaga

PII: S1549-9634(20)30168-4

DOI: https://doi.org/10.1016/j.nano.2020.102314

Reference: NANO 102314

To appear in: *Nanomedicine: Nanotechnology, Biology, and Medicine*

Revised date: 17 September 2020

Please cite this article as: Y. Polo, J. Luzuriaga, J. Iturri, et al., Nanostructured scaffolds based on Bioresorbable polymers and Graphene oxide induce the aligned migration and accelerate the neuronal differentiation of neural stem cells, *Nanomedicine: Nanotechnology, Biology, and Medicine* (2020), https://doi.org/10.1016/j.nano.2020.102314

This is a PDF file of an article that has undergone enhancements after acceptance, such as the addition of a cover page and metadata, and formatting for readability, but it is not yet the definitive version of record. This version will undergo additional copyediting, typesetting and review before it is published in its final form, but we are providing this version to give early visibility of the article. Please note that, during the production process, errors may be discovered which could affect the content, and all legal disclaimers that apply to the journal pertain.

© 2020 Published by Elsevier.

Journal Pre-proof

Nanostructured Scaffolds Based on Bioresorbable Polymers and Graphene Oxide Induce the Aligned Migration and Accelerate the Neuronal Differentiation of Neural Stem Cells

Y. Polo[a$], J. Luzuriaga[b$], J. Iturri[c], I. Irastorza[b], J.L. Toca-Herrera[c], G. Ibarretxe[b], F. Unda[b], J.R. Sarasua[d], J.R. Pineda[b,e#] and A. Larrañaga[d#]

[a]Polimerbio SL, Donostia-San Sebastian, Spain.
[b]Department of Cell Biology and Histology, Faculty of Medicine and Nursing, University of the Basque Country (UPV/EHU), Leioa, Spain.
[c]Institute for Biophysics, Department of Nanobiotechnology, BOKU University of Natural Resources and Life Sciences, Vienna, Austria.
[d]Group of Science and Engineering of Polymeric Biomaterials (ZIBIO Group), Department of Mining, Metallurgy Engineering and Materials Science & POLYMAT, University of the Basque Country (UPV/EHU), Bilbao, Spain.
[e]Achucarro Basque Center for Neuroscience, University of the Basque Country (UPV/EHU), Leioa, Spain.
[$]These authors contributed equally to this work.

[#]**Corresponding Authors:** Aitor Larrañaga. Department of Mining, Metallurgy Engineering and Materials Science & POLYMAT, University of the Basque Country (UPV/EHU), Bilbao, Spain.
Telephone: +34 946 013 935
E-mail: aitor.larranagae@ehu.eus
ORCID: 0000-0002-2123-6069

Jose M. Pineda. Cell Signaling lab, University of the Basque Country (UPV/EHU), Leioa, Spain
Telephone: +34 946 013 218
E-mail: joseramon.pinedam@ehu.eus
ORCID: 0000-0002-0900-7466

Funding sources
Basque Government (GV/EJ) Department of Education, Linguistic Politics and Culture (GIC 15/52, IT-927-16), MINECO «Ramón y Cajal» program RYC-2013-13450 (JRP), MINECO PID2019-104766RB-C21, The University of The Basque Country (UPV/EHU) by GIU16/66, UFI 11/44, COLAB19/03 and IKERTU-2020.0155. GV/EJ, IT831-13, Hazitek ZE-2019/00012-IMABI and ELKARTEK KK-2019/00093. Polimerbio and Y. P. have a Bikaintek PhD grant (20-AF-W2-2018-00001) and J.L. has a UPV/EHU grant DOKBERRI 2019 (DOCREC19/49).

Conflict of interest
The authors declare that there is no conflict of interest.

Word Count-Abstract: 143
Word Count-Manuscript (body text + figure legends): 5629
Number of Figures: 9
Number of References: 60

Abstract

Within the field of neural tissue engineering, there is a huge need for the development of materials that promote the adhesion, aligned migration and differentiation of stem cells into neuronal and supportive glial cells. In this study, we have fabricated bioresorbable elastomeric scaffolds combining an ordered nanopatterned topography together with a surface functionalization with graphene oxide (GO) in mild conditions. These scaffolds allowed the attachment of murine neural stem cells (NSCs) without the need of any further coating of its surface with extracellular matrix adhesion proteins. The NSCs were able to give rise to both immature neurons and supporting glial cells over the nanostructured scaffolds *in vitro*, promoting their aligned migration in cell clusters following the nanostructured grooves. This system has the potential to reestablish spatially oriented neural precursor cell connectivity, constituting a promising tool for future cellular therapy including nerve tissue regeneration.

Keywords

Micro- and nanopatterning, neural stem cells, migration, cell differentiation, graphene oxide, biodegradable polymer.

Journal Pre-proof

Background

Regeneration of the nervous system still remains very challenging due to its limited plasticity and poor ability to heal and recover its function after injury.[1] Hence, further research is necessary to develop effective strategies for a guided neural regeneration and reestablishment of the lost nerve connectivity.

Within the field of neural tissue regeneration, the discovery and/or optimization of biomaterials that fulfill the complex requirements for this specific biomedical application play a pivotal role. Much progress has been made in determining the ideal features a biomaterial should have for its use as a neural replacement graft, and in understanding the interactions of growing axons within these biomaterials; however, the regeneration levels induced by the biomaterial usually do not match those obtained by nerve tissue autografts and the development of new and effective nerve regeneration therapies is still an urgent clinical need.[2,3]

The biomaterials for nerve tissue regeneration should be biocompatible and biodegradable, while providing structural cues that promote oriented axon regeneration and guidance signals from extracellular matrix (ECM)-like components. Additionally, they should also present long-term storage capability and ease of handling/suturing.[4–6] One important aspect to take in consideration is that the ECM is more than just a structural component. Indeed, for stem cells in particular, both the topography and composition of the ECM are pivotal in instructing cell fate choices by selective contact guidance, promotion of cell adhesion and concentration of growth factors and/or signaling ligands to defined niches.[7] However, negative effects produced by an inappropriate choice of ECM can also be identified. For instance, an excess of the typically employed ECM adhesion protein laminin $\alpha_2\beta_2\gamma_1$ (Lm211) can inhibit signaling

pathways required to initiate myelination.[8] Furthermore, laminin ECM proteins may represent a lethal risk if at some point resident and/or grafted cells became cancerous. It has been demonstrated that laminin primes the proliferation of brain tumor cells such as ependymoma or glioblastoma cancer stem cells, becoming strongly correlated to negative patient prognosis.[9] For all these reasons, it is urgent to design a biomaterial scaffold with the ability to allow the attachment of neural stem cells and progenitors without the need of a laminin coating.

To overcome these challenges, the use of polymeric substrates that mimic the mechanical (e.g., elasticity, stiffness), geometrical and chemical features of the ECM has been described to satisfactorily promote the differentiation of stem cells towards neural lineages.[10] Among the available polymeric substrates, bioresorbable (co)polyesters based on L-lactide and ε-caprolactone are of particular interest. These systems show inherent biodegradability, biocompatibility and the possibility to tune the mechanical properties and degradation rates depending on the specific application, via the precise control of the L-lactide-to-ε-caprolactone ratio and synthesis conditions (e.g., catalyst, reaction temperature and time).[11–13] Nevertheless, nowadays, polymeric devices are not just bioinert support materials for cell growth. To fit within the new discipline of materiobiology,[14] they also need to mimic the morphological, topographical and mechanical properties of the desired tissue.[15] To fulfill these requisites, nanopattern construction represents a promising strategy to endow the material surface with specific geometrical and mechanical signals. Nanopatterns can potentially elicit a stem cell response, as surface nanotopography could induce pronounced changes to cell shape, and consequently also in gene expression.[16] In this regard, the importance of nanotopography was shown on the differentiation of adult stem cells towards neuronal lineages, compared to unpatterned and micro-patterned

control surfaces.[17] Moreover, the combination of nanotopography with graphene derivatives (e.g., graphene oxide (GO), reduced graphene oxide (rGO)) has been shown to promote neuronal differentiation and axon alignment.[18] In the recent years, GO-based materials have been extensively explored as some of the most promising biomaterials for neural regeneration[19] thanks to their unique properties.[20]

However, there is still much to investigate regarding the impact of nanotopography and graphene derivatives on the mobility of the cells along the scaffold device, the *in situ* differentiation of stem cells into glial or neuronal cells and the necessary equilibrium between both pathways, to achieve a functional recovery of the neural tissue. Therefore, we have developed novel two-dimensional nanostructured tissue engineering scaffolds based on bioresorbable polymers and GO as a new alternative to promote the neurodifferentiation of murine neural stem cells (NSCs) and progenitors, which are competent to give rise to both mature neuronal and glial cells. The high efficiency shown by these nanopatterned scaffolds, even under long incubation periods compatible with usual differentiation protocols, turns them into an optimal and easy-to-produce tool.

Methods

Fabrication of scaffolds

PURASORB PLC 7015 (Corbion, The Netherlands) (PLCL 7015) is a biodegradable copolymer of L-lactide and ε-caprolactone in a 70/30 molar ratio, with a weight average molecular weight (M_w) of 154.6 kDa and dispersity index (DI) of 2.10, as determined by gel permeation chromatography (GPC). For the fabrication of the scaffolds, PLCL films of around 150 μm were first obtained by compression moulding

in a Collin P 200 E (Germany) hydraulic press at 175 ºC. These films were subsequently nanostructured by a thermo-pressing process at 190 ºC and 20 N with the aid of a commercially available silicon stamp (NIL Technology, Denmark) (period: 700 nm; linewidth: 365 nm; depth: 350 nm) (Supplementary Figure 1). For the surface-functionalization with GO, the nanostructured PLCL scaffolds were incubated in a 2 mg/ml dopamine-hydrocholoride (cat# H8502, Sigma-Aldrich, Spain) solution in 2-amino-2-(hydroxymethyl)-1,3-propanediol (TRIS) buffer (cat# T1503, Sigma-Aldrich, Spain) at pH = 8.5 for 1 h to form a homogeneous layer of polydopamine (PDA). To eliminate the excess of PDA and reagents, the films were thoroughly washed with distilled water. Afterwards, PDA-coated films were incubated in a 0.25 mg/ml GO solution (cat# 947-768-1, Graphenea, Spain) for 30 min to allow the deposition of GO on the surface of the nanostructured scaffolds. Finally, the scaffolds were extensively washed with distilled water prior to their use and characterization. Circular samples of 6 mm diameter were punched out for subsequent characterization and cell culture studies. Details about the morphological and physico-chemical characterization of the scaffolds can be found in the supplementary material.

Cell culture

NSCs were obtained, cultured in Neurocult proliferation media and passaged as previously described.[7,21] Cells were seeded at a density of either 5,000 cells to quantify cell and leading-edge orientation or 10,000 cells per scaffold for differentiation purposes. For the control assays, NSCs were seeded onto 12 mm coverslips either coated with laminin or non-coated (L2020, Sigma, St. Louis, MO), as previously described.[22] Cell differentiation was induced using Neurocult differentiation supplement (cat# 05752, Stem Cell Technologies, Vancouver, Canada) at 9:1 ratio, 2% B27

supplement (cat# 17504044, Gibco, Waltham, MA USA), in the presence of 100 U/ml penicillin and 150 µg/ml streptomycin antibiotics. Fresh medium was replaced every three days. Cell orientations were calculated by measuring the orientation angle of the leading edge relative to a common reference point using ImageJ software. Further detailed information about experimental procedure of cell cultures, immunostaining protocols as well as scanning electron microscopy (SEM) observations and videorecording[23] of NSCs can be found in the supplementary material section.

Statistical methods

Comparisons between multiple groups were made using Kruskal-Wallis followed by Dunn´s post hoc test or Holm-Sidak method. In turn, comparisons between only two groups were made using U-Mann Whitney test, where $p<0.05$ was considered as statistically significant. Results were presented as mean ± standard deviation (SD) or standard error mean (SEM) (indicated accordingly). The number of independent experiments is shown in the respective figure legend. For the mechanical properties of the samples via atomic force microscopy (AFM), the statistical difference between groups was tested by *t*-test and two-way analysis of variance (ANOVA) at a confidence level of 95% ($p<0.05$).

Results

PLCL scaffolds are successfully fabricated, nanostructured and functionalized

The topography of the silicon stamp was faithfully replicated on the PLCL films, yielding nanostructured PLCL scaffolds with a well-defined grooved pattern (Figure 1, *A*). The surface of the scaffolds was characterized by ridges of 496.5±29.8 nm and grooves of 203.3±22.8 nm. For a more detailed morphological characterization, atomic

force microscopy (AFM) was employed (Figure 1, *B*). As evidenced from these images, some ridges appeared slightly distorted, which can be ascribed to the soft mechanical behavior of this polymer at room temperature.[24] The subsequent surface functionalization with PDA did not have any detrimental effect on the observed nanotopography (Figure 1, *A* and *B*). The concentration of the initial dopamine hydrochloride solution and the reaction time were carefully controlled to avoid the excessive deposition of PDA agglomerates that could deteriorate the native nanostructured topography of the scaffolds (Supplementary Figure 3, *A*). This nanostructured topography was also preserved after the final functionalization with GO (Figure 1, *A* and *B*). Working at higher GO concentrations in this step resulted in the excessive deposition of GO, which, again, covered some areas of the polymeric film (Supplementary Figure 3, *B*). In the case of non-nanostructured PLCL scaffolds (Supplementary Figure 4, *A* and *B*), a slight increase in the overall roughness was observed as PDA and GO were deposited, similar to the results observed for the nanostructured scaffolds.

To confirm the successful functionalization of the scaffolds with PDA and GO, the samples were subjected to X-ray photoelectron spectroscopy (XPS), Raman spectroscopy and AFM in force spectroscopy mode analysis. After PDA coating, an increase (from 29 to 41%) of the contribution at 285.0 eV, that corresponds to C-C/C-H bonds, was observed in the C 1s spectrum with respect to the pristine PLCL scaffold (Figure 2, *A*). Additionally, in the N 1s spectra a peak centered at 400.0 eV appeared, which can be ascribed to secondary and primary amine groups, and imine functionalities from PDA. The differences in the XPS spectra after surface functionalization with GO with respect to PDA-coated films was negligible and only a slight decrease (from 3.1 to 1.6%) in the nitrogen signal was detected.

Raman spectroscopy however, truly confirmed the presence of GO on the surface of the PLCL scaffolds (Figure 2, *B*). The intensities of the D and G bands, which are associated respectively to the disordered structure of graphene in sp^2-hybridized carbon and stretching of the C-C bond in graphitic materials,[25] increased with the concentration of the employed GO solution for the incubation. Note that the D and G bands were not present in the scaffold incubated with a 0.25 mg/ml GO solution but in the absence of PDA adlayer, which highlights the importance of the PDA coating for the successful functionalization of the surface with GO. Subsequent experiments were performed with the scaffolds functionalized with a GO concentration of 0.25 mg/ml, which ensured a successful surface functionalization while preserving the native nanotopography of the PLCL scaffolds.

The employment of AFM in force spectroscopy mode enabled the quantitative evaluation of the mechanical properties (adhesion) at the interface between cells and the substrate. As can be observed in Figure 2, *C*, hydrophobic probes led to larger forces than fibronectin-coated ones (used as control), independently of the substrate under analysis. For the hydrophobic probes, the maximum adhesion value, together with the corresponding adhesion work, decreased with the different coatings applied (Supplementary Table 1). This could be explained by the higher hydrophobic character of PLCL (water contact angle-WCA ~ 90-100º), in comparison with thin PDA (WCA ~ 50º), GO (WCA ~ 15-30º) and laminin (< 10º) films which were gradually more hydrophilic. This behavior highlights the fact that level-wise modification of PLCL took place satisfactorily, and that just a few nanometers are enough to change the character of the interface.

For fibronectin-coated colloids, and despite the much lower values calculated, the different content of the substrate also led to a variation in the adhesion-related

response. In this case, forces of hydrophobic nature were not the dominant ones anymore. Indeed, adhesion factors for bare PLCL suffered a 10-fold drop in comparison with hydrophobic probe measurements (Figure 2, *C* and Supplementary Table 1). Here, PDA-coated scaffolds appeared as the predominant ones while those containing GO on top presented lower affinity for fibronectin, although still higher than control laminin films. Therefore, the effective action of the surface modification is again confirmed.

Neural stem cells and progenitors attach and align following nanopattern shape without the need of a laminin coating

Laminin has been extensively used for monolayer coating of NSC cultures. To test whether NSCs were able to adhere and survive to surfaces without laminin coating, 5,000 NSCs were seeded onto nanostructured scaffolds functionalized with GO (NanoGO), which is reported to promote cell adhesion and neuronal differentiation thanks to its physico-chemical features,[11,15] or without GO (NanoPDA). After initial seeding, a time-course was carried out observing how 10 min on laminin was enough for cell attachment, whereas 45 min were needed on nanostructured scaffolds. Progressively, those cells seeded on nanostructured scaffolds created aligned paths of migration becoming evident at 24 h. On the contrary, cells seeded on laminin kept a randomized aleatory orientation (Supplementary figure 5). So, 45 min after initial seeding, attached cells on only nanostructured surfaces showed an aligned cell-body orientation evidenced by the cell shape (Figure 3, *A*). We noticed that this orientation could follow the surface nanopattern (Figure 3, A Supplementary Figure 5). A quantification representing the variation of angle measurements was performed and determined that 70% of the cells were perfectly aligned with NanoGO, meanwhile NanoPDA showed a 67% of cells aligned with a variation of 30º. Non-nanostructured

scaffolds had shorter leading edge processes with no preferential orientation (Figure 3, *B*). Two hours post-seeding, the length of the leading cellular process was determined. The cells seeded on NanoGO showed the maximal elongation with an average of 32.45±6.74 µm while NanoPDA showed a reduced length of 23.66±5.41 µm. On the contrary, the leading processes of the cells seeded on non-nanostructured scaffolds functionalized with GO (No NanoGO) were smaller than without the functionalization (No NanoPDA) (13.74±1.29 and 23.86±9.19 µm respectively; $p<0.001$ ANOVA, Supplementary Figure 6).

To test whether nanostructured scaffolds were able to guide the orientation and migration of NSCs for longer periods that are compatible with neuronal differentiation protocols, the experiment was repeated by allowing the seeded NSCs to grow for three days *in vitro* (DIV3) in proliferation medium. Afterwards, the culture medium was changed to differentiation medium to allow cellular neurodifferentiation. The culture was kept for another seven days (total DIV10, Figure 4, *A*). As previously observed during 24 h (Supplementary Figure 5), the nanostructured materials induced an oriented growth and migration of NSCs along the parallel grooves during the initial three days of culture, independently of the GO functionalization. Non-nanostructured surfaces only showed large spheroid-shaped cellular structures as in (non-coated glass control) standard free-floating neurosphere cultures (Figure 4, *B*). To further confirm the results and corroborate that 1) cells were aligning according to the nanograting axis and 2) the alignment could be maintained after cell differentiation, cells were seeded and allowed to attach in proliferation medium for 24 h. Thereafter, the medium was changed to induce cell differentiation and cells were fixed at DIV7 or DIV14. SEM analysis demonstrated the alignment of cell clusters following the nanostructured grooves both at DIV7 (Supplementary Figure 7, *A*) and DIV14 (Supplementary Figure 7, *B*). Thus,

NSCs grew aligned with the surface nanopattern in a timescale compatible with neural cell differentiation protocols.

Surface nanostructured grooves allow the oriented migration of neural stem and progenitor cells

Since cell migration is a critical factor for complete tissue regeneration (e.g., wound healing), the next step was to assess the dynamics of cell growth and adhesion over the different biomaterials. Hence, NSCs were seeded on the scaffolds and videorecorded for 72 h to characterize its migratory properties. Cells cultured over nanostructured scaffolds independently on the functionalization with GO (NanoPDA vs. NanoGO) displayed a lower motility with respect to cells cultured over laminin (mean velocity of 12.67±1.54 μm/h (NanoPDA), 15.23±1.17 μm/h (NanoGO) and 26.49±0.68 μm/h (laminin control)), ($p<0.001$ One-way ANOVA, Figures 5, *A* and *B* and Supplementary Video 1). Remarkably, the difference between GO presence and GO absence conditions was not statistically significant ($p<0.075$, One-way ANOVA, Figure 5, *B*). Persistence time characterizes the average time between significant changes in the direction of a translocation of a cell.[26–28] This value allows a quantitative analysis of the differences in migration behavior. The results are shown in the percentage of time. The cells cultured on nanostructured NanoPDA and NanoGO scaffolds showed significantly more persistence than the cells cultured on laminin control (35.81±19.19% (NanoPDA) and 17.82±5.51% (NanoGO) with respect to 7.31±1.42% (laminin control)), ($p<0.001$, One-way ANOVA, Figure 5, *C*). According to these results, nanostructured scaffolds showed an increased pausing time in comparison with those coated with laminin (98.81±0.96% (NanoPDA), 97.37±0.72% (NanoGO) and 91.14±1.31% (laminin control)), ($p<0.001$, One-way ANOVA, Figure 5, *D*). Also the total traveled distance for

an interval of 8 h was similar on nanostructured scaffolds NanoPDA and NanoGO and much higher in the case of laminin control (40.79±35.89 µm (NanoPDA), 68.59±16.95 µm (NanoGO), and 316.91±45.01 µm (laminin control)), ($p<0.001$, One-way ANOVA, Figure 5, *E*).

Neural stem and progenitor cells cultured on nanostructured scaffolds are able to generate neuronal and astroglial lineage cells

Another important aspect for neural tissue cell therapy is to preserve the capabilities to generate newborn neurons as well as their supportive glial cells. To check whether nanostructured scaffolds were permissive to the generation of both neuronal and astroglial lineages, NSCs were first kept for 24 h in proliferation medium and then switched to differentiation medium. At DIV7 with differentiation medium, both nanostructured and non-nanostructured scaffolds with or without GO were fixed for immunostaining. Neuroblasts are neuronal precursors with migratory properties that strongly express the protein doublecortin (DCX).[29–31] On the other hand, astrocytes are other abundant cells in the central nervous system that abundantly express glial acidic fibrillary protein (GFAP).[32] Double immunofluorescence against DCX and GFAP showed the presence of both these cell types on the nanostructured scaffolds (Figure 6A). In the case of non-nanostructured scaffolds, due to the lack of adhesion, only few cells were counted on the immunostaining. Control cultures grown using laminin showed a homogenous non-aligned patterns of cell organization of DCX (Figure 6B).

Journal Pre-proof

Both nanotopography and GO change the profile of gene expression with respect to laminin at different times post seeding.

Laminin has been widely used as extracellular matrix component for NSC growth. Because nanostructured scaffolds and GO are alternative substrates permissive for cell attachment, we decided to compare the profile of gene expression changes between NanoGO and NanoPDA with respect to laminin at different cell culture time points. We found that both NanoGO and NanoPDA were permissive to maintain MASH-1 expressing neural progenitor cells and allowed a mild increase in the TLX neural stem cell marker at early time points (1.55±0.20 and 2.36±0.49 fold at DIV3 and DIV7 dropping to 0.83±0.07 at DIV10 (Figure 7A)). Interestingly we observed an increase of gene expression of NeuN (2.51±1.86 fold) and DCX (54.66±19.58 fold) at DIV7 in NanoPDA scaffolds, both related to neural fate (Figure 7B), together with a stable expression of the stem/astroglial marker GFAP (1.00±0.06 fold). However, the S100β, a marker of mature astrocytes, showed a delayed increase rising from 0.84±0.04 to 1.50±0.19 from DIV7 to DIV10 for NanoGO with respect to laminin control (ratio 1). These results suggested that nanostructured grooves were able to induce significant changes on the profile of gene expression with respect to laminin during the progression of the cell culture. Notably, the rate of expression of neuronal markers (DCX, NeuN) was higher in NSCs seeded over NanoGO and NanoPDA at intermediate time points (DIV7).

NSC differentiation to astroglial lineage is accelerated by the presence of both nanostructured grooves and GO

To contrast the information provided by gene expression profiles, we decided to check both protein expression and cell fate by immunofluorescence over cells on

nanopatterned surfaces. NSCs cultured with differentiation medium on laminin-coated coverslips progressively differentiate towards mature astroglial fates over time (Figure 8). The level of glia maturation can be determined as follows: i) immunostaining for GFAP and the absence of S100β (immature glia), ii) the presence of both markers (maturing glia) and iii) the absence of GFAP and presence of S100β (fully mature glia). In control (laminin-coating) conditions, GFAP positive cells increased over time from 0.64±0.13% at DIV3 to 28.35±3.13% at DIV10 ($p<0.005$, One-way ANOVA) (Figure 8). These cells also presented a more intense GFAP+ staining with longer differentiation time. On the other hand, S100β+ staining did not present such variation with values of 20.97±1.48% at DIV3 and 28.60±7.07% at DIV10 ($p>0.99$, One-way ANOVA). But the maturing glia presenting GFAP and S100β double stain, increased from 0.32±0.08% to 7.92±1.27% from DIV3 to DIV10, showing the maturation of the cells over time ($p<0.05$, One-way ANOVA). The astroglial differentiation of cells seeded on the nanostructured scaffolds showed a remarkable increase on the amount of GFAP positive cells at DIV3 with respect to laminin. NanoPDA 75.25±4.10%, NanoGO 99.02±8.58%, laminin control 0.64±0.13% ($p<0.05$, One-way ANOVA). Therefore, both the nanopatterning and the presence of GO seemed to shorten the onset of the glial differentiation of NSCs. Also, the percentage of S100β+ increased in all the scaffolds tested at DIV3 with respect to laminin control: NanoPDA 35.84±2.33%, NanoGO 71.94±4.37% and laminin control 20.97±1.48% ($p<0.05$, One-way ANOVA). Again, this quick maturation was more remarkable on the nanostructured scaffolds functionalized with GO. The amount of GFAP+/S100β+ double stained cells was also higher on the nanostructured scaffolds tested, with respect to laminin control at DIV3: NanoPDA 33.96±2.37%, NanoGO 70.94±6.37% and laminin control 0.32±0.08% ($p<0.05$, One-way ANOVA).

It is also worth mentioning that the nanostructured scaffolds functionalized with GO, even though they showed the fastest glial differentiation, presented a reduced amount of GFAP+, S100β+ and GFAP+/S100β+ double positive population at DIV7 (GFAP+ 12.07±1.83%; S100β+ 0.25±0.10%; GFAP+/S100β+ 0.25±0.10%) ($p<0.05$, One-way ANOVA) and DIV10 (GFAP+ 4.33±0.50%; S100β+ 18.68±1.29%; GFAP+/S100β+ 2.98±0.43%) ($p<0.05$, One-way ANOVA) with respect to the values observed at DIV3 (GFAP+ 99.02±8.58%; S100β+ 71.94±4.37%; GFAP+/S100β+ 70.94±6.37%). On the other hand, the NanoPDA scaffolds also presented a lower population (5.89±0.20%) of GFAP+ positive cells at DIV10 compared to laminin control (28.35±3.13%) ($p<0.05$, One-way ANOVA).

NSC differentiation to neuronal lineage is enhanced by the combination of nanostructured grooves and GO

NSCs cultured with differentiation medium on laminin-coated coverslips progressively differentiate towards mature neuronal fates over time, losing DCX and expressing instead NeuN (Figure 9). The level of neuronal maturation was determined by: i) immunostaining for DCX and the absence of the nuclear neuronal marker NeuN (immature neurons), ii) the presence of both markers (maturing neurons) and iii) the absence of DCX and presence of NeuN (fully mature neurons). In control laminin-coating conditions, the DCX positive cell population dropped significantly from 30.85±2.41% at DIV7 to 15.90±0.02% at DIV10 ($p<0.05$, One-way ANOVA). The percentage of maturing neurons co-expressing DCX+/NeuN+ was of 15.66±3.31% and 14.46±2.05% for DIV7 and DIV10, respectively ($p<0.108$, One-way ANOVA). When we turned to evaluate mature cell differentiation over scaffolds, we found an enhanced neurodifferentiation of the cells on NanoPDA and NanoGO compared to laminin

control. We found that both NanoGO and NanoPDA scaffolds increased the amount of NeuN+ positive cells at DIV10, compared to laminin control (NanoGO 90.41±0.20, NanoPDA 96.72±3.06% and laminin control 28.62±1.30%). Furthermore, NanoGO scaffolds increased the number of NeuN+ positive cells with respect to both laminin control and NanoPDA at DIV7 (NanoGO 52.50±0.04%; NanoPDA 3.2±0.01% and laminin control 18.46±3.20%) ($p<0.05$, One-way ANOVA), thus considerably shortening the time needed for complete neuronal differentiation (Figure 9). Remarkably, PDA-coated scaffolds (NanoPDA) were enough to increase DCX+ (49.10±1.47%) and NeuN+ (96.72±3.05%) cell populations at DIV10 even without a need of neither laminin nor GO compared to laminin ($p<0.05$, One-way ANOVA). The number of neurons co-expressing DCX+/NeuN+ was significantly increased on the NanoPDA scaffolds at DIV10, with respect to NanoGO and laminin control (NanoPDA 49.18±0.03%; NanoGO 24.08±0.02% and laminin control 14.46±2.05%), ($p<0.05$, One-way ANOVA). Overall, NanoGO scaffolds seemed to accelerate the most the NSC differentiation into neuronal pathway.

Discussion

In the present study, we characterized a nanostructured scaffold able to support the oriented alignment, growth, migration and differentiation of neural stem and progenitor cells. Although the use of nanostructured scaffolds as a tool to promote cell alignment and differentiation is well reported in bibliography from a conceptual perspective, most of the studies either employ non-biodegradable substrates or complex procedures for the fabrication of the scaffolds, which enormously limit their potential in the biomedical field.[16,33–36] Besides, the fabrication and post-functionalization processes are frequently performed in the presence of organic solvents that may induce a cytotoxic

effect if they are not completely eliminated.[37] Herein, we employed a fully bioresorbable, FDA-approved polymeric material based on L-lactide and ε-caprolactone (70/30 molar ratio).[38] This copolymer undergoes a random-scission of its ester linkages in aqueous solutions and starts losing weight after approximately 80 days in PBS.[39] Considering also that, in the bulk degradation process, the degrading chains are not expelled out to the surrounding environment until the end of the degradation process,[40] we do not expect any interference of the degradation by-products with the cell differentiation process studied herein. Thanks to its thermoplastic nature, the nanotopography of a commercially available silicon stamp was easily and quickly replicated on the polymeric film without the need of any organic solvent or complex processes, which highlights the robustness, scalability and versatility of this methodology. Following this solvent-free strategy, the post-functionalization of the nanostructured scaffolds was achieved by exploiting the multiple interactions between PDA and virtually any substrate in slightly basic aqueous solutions.[41] First, the nanostructured scaffolds were coated with a thin and homogeneously distributed layer of PDA that preserves the native nanotopography of the original films. The PDA coating played a pivotal role in the subsequent functionalization with GO as demonstrated by the absence of GO on the surface of the scaffolds when PDA was not employed as an adlayer. This can be associated to several interactions between PDA and GO, including hydrogen bonding between amine and hydroxyl groups of PDA and GO respectively and π-π stacking between catechol groups of PDA and the hexagonal lattice of GO.[42]

The properties of these scaffolds offer the advantage of NSC adhesion without the need of a laminin coating. Additionally, the nanostructured scaffolds NanoGO and NanoPDA offered the advantage of cell alignment and elongation along the nanostructured grooves. Even though the induction of cell alignment and elongation

according to a determined nanograting axis has been reported before,[16,43,44] we found that nanostructured scaffolds also allowed the directionality of cell migration along the nanostructured grooves. Thus, our strategy goes a step further allowing the possibility of creating migration paths of NSCs and their differentiated cell progeny that follow a determined orientation according to the desired nanopatterning.

Another important aspect to take in consideration is the effect of the scaffolds to enhance and accelerate neural differentiation. We found that nanostructured scaffolds are able to induce cell differentiation towards both neuronal and astroglial lineages. Moreover, they are able to induce the differentiation towards neuronal lineages at earlier times than those of the ECM adhesion protein laminin. The induction of neurodifferentiation of stem cells thanks to a synthetic nanostructure has been previously reported.[17] Besides, we found an increase on GFAP+ positive cells at early stages in the nanostructured scaffolds NanoPDA and NanoGO. It has been reported before the positive GFAP staining of NSCs cultured from postnatal mouse forebrains,[45] so these results may indicate the presence of undifferentiated NSCs in the culture at DIV3 and 7 on the scaffolds. The amount of S100β+ positive cells is also increased at DIV3 in NanoGO scaffolds and at DIV7 on NanoPDA scaffolds compared to laminin control. Interestingly, S100β is expressed in both mature astroglia and early oligodendrocyte precursor cells.[46,47] In agreement with previous works, we cannot exclude the possibility of S100β+ oligodendroglial cells at DIV3 on NanoGO scaffolds compared to NanoPDA.[48]

On the other hand, it has been previously reported that the presence of GO enhances cellular neurodifferentiation,[49] while the combination of GO with electrical stimulation induces NSC proliferation, neuronal differentiation and neurite elongation.[43] Although GO has been widely chosen instead of pure graphene due to its better

capability for laminin assembly, not much data has been reported for the effects of GO-coated scaffolds without the use of ECM-like intermediates.[50,51] We found that laminin-free NanoGO scaffolds reduced the time cells need to express neuronal markers with respect to standard laminin coating and NanoPDA scaffolds. Thus, both nanopatterning and GO surface functionalization can be combined to enhance and accelerate neuronal differentiation. In agreement with our results, other works claimed that nanostructured rGO microfibers were able to offer an alternative substrate for NSC adhesion when compared with 2D graphene films, and an increasing neuronal differentiation but with only few astroglial cells surrounding the microfibers.[52] In agreement with this work of Guo et al., we observed that neuronal differentiation was boosted at DIV7 on the NanoGO scaffolds, at the expense of the astroglial population. However, it is well reported in literature that glial cells are necessary to support neuronal cells.[53–56] Astrocytes for example, cooperate with neurons on several levels, including neurotransmitter trafficking and recycling, ion homeostasis, energy metabolism, and defense against oxidative stress.[57,58] Consequently, this faster differentiation may provoke a mid-term reduction of viability probably by changes of compensatory proportions of neurons and astroglial support. Following the same reasoning, GO has also been previously reported as a potential cytotoxic agent in chicken embryos.[59,60] However, we have not found a variation of apoptotic/pycnotic nuclei in immunostainings experiments, neither retracting cell process nor cell blebbing after SEM examination. This fact reinforces the arguments for the potential clinical use of these nanopatterned scaffold systems.

Journal Pre-proof

Acknowledgments

We would like to thank Jorge Fernandez (Polimerbio SL) for the support in this project. SGIker technical services (UPV/EHU) are gratefully acknowledged for XPS and Raman support. We would like to thank Ricardo Andrade and Alejandro Díez, responsible of the High-Resolution Analytical Microscopy Service in Biomedicine (SGIker UPV/EHU), for their invaluable help for the electron microscopy and cell videorecording assistance. We would like to thank Laura Escobar for confocal microscopy in the Achucarro Basque Center for Neuroscience Fundazioa and Fabrice Cordelières (Bordeaux Imaging Center) for the macro developed for ImageJ.

References

1 Ahuja C. S., Nori S., Tetreault L., Wilson J., Kwon B., Harrop J. et al, Traumatic spinal cord injury-repair and regeneration, Neurosurgery. 2017, **80**:S9–S22. https://doi.org/10.1093/neuros/nyw080.

2 Gu X., Ding F., Yang Y., Liu J., Construction of tissue engineered nerve grafts and their application in peripheral nerve regeneration, Prog. Neurobiol. 2011, **93**:204–230. https://doi.org/10.1016/j.pneurobio.2010.11.002.

3 Rajaram A., Chen X. B., Schreyer D. J., Strategic design and recent fabrication techniques for bioengineered tissue scaffolds to improve peripheral nerve regeneration, Tissue Eng. Part B Rev. 2012, **18**:454–467. https://doi.org/10.1089/ten.TEB.2012.0006.

4 Deumens R., Bozkurt A., Meek M. F., Marcus M. A. E., Joosten E. A. J., Weis J. et al, Repairing injured peripheral nerves: bridging the gap, Prog. Neurobiol. 2010, **92**:245–276. https://doi.org/10.1016/j.pneurobio.2010.10.002.

5 Kehoe S., Zhang X. F., Boyd D., FDA approved guidance conduits and wraps for peripheral nerve injury: a review of materials and efficacy, Injury. 2012, **43**:553–572. https://doi.org/10.1016/j.injury.2010.12.030.

6 Spivey E. C., Khaing Z. Z., Shear J. B., Schmidt C. E., The fundamental role of subcellular topography in peripheral nerve repair therapies, Biomaterials. 2012, **33**:4264–4276. https://doi.org/10.1016/j.biomaterials.2012.02.043.

7 Pineda J. R., Daynac M., Chicheportiche A., Cebrian-Silla A., Felice K. S., Garcia-Verdugo J. M. et al, Vascular-derived TGF-β increases in the stem cell niche and perturbs neurogenesis during aging and following irradiation in the adult mouse brain, EMBO Mol. Med. 2013, **5**:548–562. https://doi.org/10.1002/emmm.201202197.

8 Ghidinelli M., Poitelon Y., Shin Y. K., Meroso D., Williamson C., Ferri C. et al, Laminin 211 inhibits protein kinase A in Schwann cells to modulate neuregulin 1 type III-driven myelination, PLoS Biol. 2017, **15**:e2001408. https://doi.org/10.1371/journal.pbio.2001408.

9 Lathia J. D., Li M., Hall P.E., Gallagher J., Hale J.S., Wu Q. et al, Laminin alpha 2 enables glioblastoma stem cell growth, Ann. Neurol. 2012, **72**:766–778. https://doi.org/10.1002/ana.23674.

10 Zhang S., Ma B., Liu F., Duan J., Wang S., Qiu J. et al, Polylactic acid nanopillar array-driven osteogenic differentiation of human adipose-derived stem cells determined by pillar diameter, Nano Lett. 2018, **18**:2243–2253. https://doi.org/10.1021/acs.nanolett.7b04747.

11 Ramot Y., Nyska A., Markovitz E., Dekel A., Klaiman G., Zada M. H. et al, Long-term local and systemic safety of poly(l-lactide-co-epsilon-caprolactone) after

subcutaneous and intra-articular implantation in rats, Toxicol. Pathol. 2015, **43**:1127–1140. https://doi.org/10.1177/0192623315600275.

12 Fernández J., Larrañaga A., Etxeberria A., Sarasua J. R., Effects of chain microstructures and derived crystallization capability on hydrolytic degradation of poly(l-lactide/ε-caprolactone) copolymers, Polym. Degrad. Stab. 2013, **98**:481–489. https://doi.org/10.1016/j.polymdegradstab.2012.12.014.

13 Fernández J., Larrañaga A., Etxeberria A., Wang W., Sarasua J. R., A new generation of poly(lactide/ε-caprolactone) polymeric biomaterials for application in the medical field, J. Biomed. Mater. Res. A. 2014, **102**:3573–3584. https://doi.org/10.1002/jbm.a.35036.

14 Li Y., Xiao Y., Liu C., The horizon of materiobiology: a perspective on material-guided cell behaviors and tissue engineering, Chem. Rev. 2017, **117**:4376–4421. https://doi.org/10.1021/acs.chemrev.6b00654.

15 Mohammed D., Versaevel M., Bruyère C., Alaimo L., Luciano M., Vercruysse E., Innovative tools for mechanobiology: unraveling outside-in and inside-out mechanotransduction, Front. Bioeng. Biotechnol. 2019, **7**:162. https://doi.org/10.3389/fbioe.2019.00162.

16 Silantyeva E. A., Nasir W., Carpenter J., Manahan O., Becker M. L., Willits R. K., Accelerated neural differentiation of mouse embryonic stem cells on aligned GYIGSR-functionalized nanofibers, Acta Biomater. 2018, **75**: 129–139. https://doi.org/10.1016/j.actbio.2018.05.052.

17 Yim E. K., Pang S. W., Leong K. W., Synthetic nanostructures inducing differentiation of human mesenchymal stem cells into neuronal lineage, Exp. Cell Res. 2007, **313**:1820–1829. https://doi.org/10.1016/j.yexcr.2007.02.031.

18 Solanki A., Chueng S. T. D., Yin P. T., Kappera R., Chhowalla M., Lee K. B., Axonal alignment and enhanced neuronal differentiation of neural stem cells on graphene-nanoparticle hybrid structures, Adv. Mater. Deerfield Beach Fla. 2013, **25**:5477–5482. https://doi.org/10.1002/adma.201302219.

19 Baek S., Oh J., Song J., Choi H., Yoo J., Park G. Y. et al, Generation of Integration-Free Induced Neurons Using Graphene Oxide-Polyethylenimine, Small. Ger. 2017, **13**:1601993. https://doi.org/10.1002/smll.201601993.

20 Bramini M., Alberini G., Colombo E., Chiacchiaretta M., DiFrancesco M. L., Maya-Vetencourt J. F. et al, Interfacing graphene-based materials with neural cells, Front. Syst. Neurosci. 2018, **12**: 1662-5137. https://doi.org/10.3389/fnsys.2018.00012.

21 Luzuriaga J., Pastor-Alonso O., Encinas J. M., Unda F., Ibarretxe G., Pineda J. R., Human dental pulp stem cells grown in neurogenic media differentiate into endothelial cells and promote neovasculogenesis in the mouse brain, Front. Physiol. 2019, **10**:347. https://doi.org/10.3389/fphys.2019.00347.

22 Silvestre D. C., Pineda J. R., Hoffschir F., Studler J. M., Mouthon M. A., Pflumio F. et al, Alternative lengthening of telomeres in human glioma stem cells, Stem Cells. 2011, **29**:440–51. https://doi.org/10.1002/stem.600.

23 Cordelières F. P., Petit V., Kumasaka M., Debeir O., Letort V., Gallagher S. J. et al, Automated cell tracking and analysis in phase-contrast videos (iTrack4U): development of Java software based on combined mean-shift processes, PLoS ONE. 2013, **8**:81266. https://doi.org/10.1371/journal.pone.0081266.

24 Fernández J., Etxeberria A., Ugartemendia J. M., Petisco S., Sarasua J. R., Effects of chain microstructures on mechanical behavior and aging of a poly(L-lactide-co-

ε-caprolactone) biomedical thermoplastic-elastomer, J. Mech. Behav. Biomed. Mater. 2012, **12**:29–38. https://doi.org/10.1016/j.jmbbm.2012.03.008.

25 Wu J. B., Lin M. L., Cong X., Liu H. N., Tan P. H., Raman spectroscopy of graphene-based materials and its applications in related devices, Chem. Soc. Rev. 2018, **47**:1822–1873. https://doi.org/10.1039/C6CS00915H.

26 Dunn G. A., Characterising a kinesis response: time averaged measures of cell speed and directional persistence, Agents Actions. Suppl. 1983, **12**:14–33. https://doi.org/10.1007/978-3-0348-9352-7_1.

27 Othmer H. G., Dunbar S. R., Alt W., Models of dispersal in biological systems, J. Math. Biol. 1988, **26**:263–298. https://doi.org/10.1007/bf00277392.

28 Gail M. H., Boone C. W., The locomotion of mouse fibroblasts in tissue culture, Biophys. J. 1970, **10**:980–993. https://doi.org/10.1016/S0006-3495(70)86347-0.

29 van Strien M. E., van den Berge S. A., Hol E. M., Migrating neuroblasts in the adult human brain: a stream reduced to a trickle, Cell Res. 2011, **21**:1523–1525. https://doi.org/10.1038/cr.2011.101.

30 Inta D., Alfonso J., von Engelhardt J., Kreuzberg M. M., Meyer A. H., van Hooft J. A., Monyer H., Neurogenesis and widespread forebrain migration of distinct GABAergic neurons from the postnatal subventricular zone, Proc. Natl. Acad. Sci. U. S. A. 2008, **105**:20994–20999. https://doi.org/10.1073/pnas.0807059105.

31 Englund U., Björklund A., Wictorin K., Migration patterns and phenotypic differentiation of long-term expanded human neural progenitor cells after transplantation into the adult rat brain, Brain Res. Dev. Brain Res. 2002, **134**:123–141. https://doi.org/10.1016/s0165-3806(01)00330-3.

Journal Pre-proof

32 Eng L. F., Ghirnikar R. S., Lee Y. L., Glial fibrillary acidic protein: GFAP-thirty-one years (1969-2000), Neurochem. Res. 2000, **25**:1439–1451. https://doi.org/10.1023/a:1007677003387.

33 Baranes K., Shevach M., Shefi O., Dvir T., Gold Nanoparticle-decorated scaffolds promote neuronal differentiation and maturation, Nano Lett. 2016, **16**:2916–2920. https://doi.org/10.1021/acs.nanolett.5b04033.

34 Lee J. M., Kang W. S., Lee K. G., Cho H. Y., Conley B., Ahrberg C. D. et al, Combinatorial biophysical cue sensor array for controlling neural stem cell fate, Biosens. Bioelectron. 2020, **156**:112125. https://doi.org/10.1016/j.bios.2020.112125.

35 Zhang S., Ma B., Liu F., Duan J., Wang S., Qiu J., Li D. et al, Polylactic acid nanopillar array-driven osteogenic differentiation of human adipose-derived stem cells determined by pillar diameter, Nano Lett. 2018, **18**:2243–2253. https://doi.org/10.1021/acs.nanolett.7b04747.

36 Bonaventura G., Iemmolo R., La Cognata V., Zimbone M., la Via F., Fragalà M. E. et al, Biocompatibility between silicon or silicon carbide surface and neural stem cells, Sci. Rep. 2019, **9**:1–13. https://doi.org/10.1038/s41598-019-48041-3.

37 Wang L., Liu Y., Fu J., Ning X., Zhang M., Jiang Z. et al, Release of methylene blue from graphene oxide-coated electrospun nanofibrous scaffolds to modulate functions of neural progenitor cells, Acta Biomater. 2019, **88**:346–356. https://doi.org/10.1016/j.actbio.2019.02.036.

38 Park J. H., Lee B. K., Park S. H., Kim M. G., Lee J. W., Lee H. Y. et al, Preparation of Biodegradable and Elastic Poly(ε-caprolactone-co-lactide) Copolymers and Evaluation as a Localized and Sustained Drug Delivery Carrier, Int J Mol Sci. 2017, **18**:671. https://doi.org/10.3390/ijms18030671.

39 Larrañaga A., Aldazabal P., Martin F.J., Sarasua J.R., Hydrolytic degradation and bioactivity of lactide and caprolactone based sponge-like scaffolds loaded with bioactive glass particles, Polym. Degrad. Stab. 2014, **110**:121–128. https://doi.org/10.1016/j.polymdegradstab.2014.08.021.

40 Larrañaga A., Lizundia E., A review on the thermomechanical properties and biodegradation behaviour of polyesters, Eur. Polym. J. 2019, **121**:109296. https://doi.org/10.1016/j.eurpolymj.2019.109296.

41 Lee H., Dellatore S. M., Miller W. M., Messersmith P. B., Mussel-inspired surface chemistry for multifunctional coatings, Science 2007, 318:426-430. https://doi.org/10.1126/science.1147241.

42 Hwang S. H., Kang D., Ruoff R.S., Shin H.S., Park Y. B., Poly(vinyl alcohol) reinforced and toughened with poly(dopamine)-treated graphene oxide, and its use for humidity sensing, ACS Nano, 2014, **8**:6739-6747. https://doi.org/10.1021/nn500524s.

43 Solanki A., Chueng S. T. D., Yin P. T., Kappera R., Chhowalla M., Lee K. B., Axonal alignment and enhanced neuronal differentiation of neural stem cells on graphene-nanoparticle hybrid structures, Adv. Mater., 2013, **25**:5477-5482. https://doi.org/10.1002/adma.201302219.

44 Pardo-Figuerez M., Martin N. R. W., Player D. J., Roach P., Christie S. D. R., Capel A. J. et al, Controlled arrangement of neuronal cells on surfaces functionalized with micropatterned polymer brushes, ACS Omega. 2018, **3**:12383–12391. https://doi.org/10.1021/acsomega.8b01698.

45 Imura T., Kornblum H. I., Sofroniew M. V., The predominant neural stem cell isolated from postnatal and adult forebrain but not early embryonic forebrain

expresses GFAP, J. Neurosci. 2003, **23**:2824–2832. https://doi.org/10.1523/JNEUROSCI.23-07-02824.2003.

46 Steiner J., Bernstein H. G., Bielau H., Berndt A., Brisch R., Mawrin C. et al, Evidence for a wide extra-astrocytic distribution of S100B in human brain, BMC Neurosci. 2007, **8**:1471-2202. https://doi.org/ 10.1186/1471-2202-8-2.

47 Deloulme J. C., Raponi E., Gentil B. J., Bertacchi N., Marks A., Labourdette G. et al, Nuclear expression of S100B in oligodendrocyte progenitor cells correlates with differentiation toward the oligodendroglial lineage and modulates oligodendrocytes maturation, Mol. Cell. Neurosci. 2004, **27**:453–465. https://doi.org/10.1016/j.mcn.2004.07.008.

48 Shah S., Yin P. T., Uehara T. M., Chueng S. T. D., Yang L., Lee K. B., Guiding Stem Cell Differentiation into Oligodendrocytes Using Graphene-Nanofiber Hybrid Scaffolds, Adv. Mater. 2014, **26**:3673–3680. https://doi.org/10.1002/adma.201400523.

49 Song J., Gao H., Zhu G., Cao X., Shi X., Wang Y., The preparation and characterization of polycaprolactone/graphene oxide biocomposite nanofiber scaffolds and their application for directing cell behaviors, Carbon. 2015, **95**:1039–1050. https://doi.org/10.1016/j.carbon.2015.09.011.

50 Bei H. P., Yang Y., Zhang Q., Tian Y., Luo X., Yan M. et al, Graphene-based nanocomposites for neural tissue engineering, Molecules. 2019, **24:**30781759. https://doi.org/10.3390/molecules24040658.

51 Fu C., Pan S., Ma Y., Kong W., Qi Z., Yang X., Effect of electrical stimulation combined with graphene-oxide-based membranes on neural stem cell proliferation and differentiation, Artif. Cells Nanomed. Biotechnol. 2019, **47**:1867–1876. https://doi.org/10.1080/21691401.2019.1613422.

52 Guo W., Qiu J., Liu J., Liu H., Graphene microfiber as a scaffold for regulation of neural stem cells differentiation, Sci. Rep. 2017, **7**:5678. https://doi.org/10.1038/s41598-017-06051-z.

53 Wilton D. K., Dissing-Olesen L., Stevens B., Neuron-glia signaling in synapse elimination, Annu. Rev. Neurosci. 2019, **42**:107–127. https://doi.org/10.1146/annurev-neuro-070918-050306.

54 He F., Sun Y. E., Glial cells more than support cells?, Int. J. Biochem. Cell Biol. 2007, **39**:661–665. https://doi.org/10.1016/j.biocel.2006.10.022.

55 Araque A., Navarrete M., Glial cells in neuronal network function, Philos. Trans. R. Soc. B Biol. Sci. (2010) **365**:2375–2381. https://doi.org/10.1098/rstb.2009.0313.

56 Barber C. N., Raben D. M., Lipid metabolism crosstalk in the brain: glia and neurons, Front. Cell. Neurosci. , 2019, **13**:212. https://doi.org/10.3389/fncel.2019.00212.

57 Bélanger M., Magistretti P. J., The role of astroglia in neuroprotection, Dialogues Clin. Neurosci. 2009, **11**:281–295.

58 Kim B. J., Choi J. Y., Choi H., Han S., Seo J., Kim J. et al, Astrocyte-encapsulated hydrogel microfibers enhance neuronal circuit generation, Adv. Healthc. Mater. 2020, **9**:1901072. https://doi.org/10.1002/adhm.201901072.

59 Sawosz E., Jaworski S., Kutwin M., Hotowy A., Wierzbicki M., M. Grodzik M. et al Toxicity of pristine graphene in experiments in a chicken embryo model, Int. J. Nanomedicine. 2014, **9**:3913–3922. https://doi.org/10.2147/IJN.S65633.

60 Chen Y., Hu X., Sun J., Zhou Q., Specific nanotoxicity of graphene oxide during zebrafish embryogenesis, Nanotoxicology. 2016, **10**:42–52. https://doi.org/10.3109/17435390.2015.1005032.

Figure Legends

Figure 1. Morphological characterization of the nanostructured scaffolds.

(A) SEM and **(B)** AFM micrographs of nanostructured PLCL (Nano), nanostructured PLCL coated with PDA (NanoPDA) and further functionalized with GO (NanoGO). **(C)** AFM 3-dimensional micrograph and **(D)** SEM cross-section micrograph of a nanostructured PLCL scaffold. Scale bars, 2 μm.

Figure 2. Surface characterization of the scaffolds.

(A) High resolution C 1s (top) and N 1s (bottom) XPS spectra of nanostructured PLCL (Nano), nanostructured PLCL coated with PDA (NanoPDA) and further functionalized with GO (NanoGO). **(B)** Raman spectra of NanoGO scaffolds at different concentrations of GO solution. **(C)** Mean adhesion force (left) and work of adhesion (right) values for FSi (white) and fibronectin-coated (grey) probes. The error bars correspond to the standard error of the mean (SEM). Statistically significant differences ($p<0.05$) were observed in all the cases, except in those indicated by n.s.

Figure 3. Neural stem cells and progenitors align along the nanostructured grooves without a need of laminin coating.

(A) Brightfield microscopy images of NSCs forty-five minutes after seeding, showing the parallel alignment of cell elongations on nanostructured scaffolds. **(B)** Distribution of cell orientation measuring angle degrees around the mean (90º) in NanoGO (78 cells analyzed), NanoPDA (45 cells), No NanoGO (31 cells) and No NanoPDA (26 cells). Scale bars, 25μm.

Journal Pre-proof

Figure 4. Neural stem cells and progenitors align following the nanostructured grooves without the need of a laminin coating.

(A) Scheme of experimental design. **(B)** Images showing the evolution of NSC cultures over the different substrates with no ECM protein coating in any of them. Cells align during the initial three days following the nanostructured grooves and do not detach during one-week differentiation. Cultures with non-nanostructured grooves grow forming cell clusters without any preferential cell alignment. Control condition using a coverslip without any ECM protein coating shows that cells do not attach growing as neurospheres. Scale bars, 100 µm.

Figure 5. Nanostructured grooves induce the guided migration and alignment of neural stem and progenitor cells.

(A) Videomicroscopy snapshots at 0, 24, 48 and 72 h post seeding in nanostructured scaffolds illustrates the dynamic process of the parallel cell alignment. On the contrary NSCs seeded on laminin-coated surfaces show a random distribution over time. **(B)** Mean cell velocity, **(C)** Cell persistence, **(D)** Pausing time and **(E)** Total traveled distance of the cells over the NanoPDA and NanoGO scaffolds compared to laminin control. Bars are shown as mean ± SEM. Dots show individual data. ***$p < 0.001$, Kruskal-Wallis One Way Analysis of Variance on Ranks. Scale bars, 50 µm.

Figure 6. Neural stem and progenitor cells cultured on nanostructured scaffolds are able to generate neuronal and astroglial precursor cells.

A) Confocal microscopy images of DCX (neuroblasts) and GFAP (astrocytes) immunostaining on nanostructured surfaces. Aligned clusters containing neuronal and glial lineage cells are observed at DIV7 after switch to differentiation medium. DAPI

was used as a counterstain for cell nuclei. **B)** Confocal microscopy images of a DIV7 cell culture on laminin coating. Non-oriented neural precursor DCX+ and homogenous cell dispersion determined by DAPI counterstaining shows non-aligned cell distribution contrary to nanostructured surfaces. Scale bar, 75µm.

Figure 7. Both nanostructured grooves and GO accelerate the expression of neuronal and glial differentiation genes.

(A) Comparison of gene expression of NSCs cultured on NanoPDA, NanoGO and laminin coated glass at DIV 3, 7 and 10 post-seeding. Expression of stemness genes (MASH1 and TLX), **(B)** neuronal differentiation genes (NeuN and DCX) and **(C)** astroglial differentiation genes (GFAP and S100β). *p<0.05 compared to laminin (gray line), Duncan´s method One Way Analysis of Variance on Ranks.

Figure 8. Both nanostructured grooves and GO accelerate the differentiation of neural stem and progenitor cells towards astroglial lineage.

(A) Double immunofluorescence for the astroglial lineage markers GFAP (red) and S100β (green) at DIV 3, 7 and 10 post-seeding in the different conditions. **(B)** Quantification of the proportion of GFAP+ **(C)** S100β+ and **(D)** GFAP+/S100β+ double stained positive cells. *p<0.05 compared to laminin. ***p<0.001 between the treatments NanoPDA and NanoGO, Holm-Sidak method One Way Analysis of Variance on Ranks. Scale bar, 50 µm.

Figure 9. Both nanostructured grooves and GO accelerate the differentiation of neural stem and progenitor cells towards neuronal lineage.

(A) Double immunofluorescence for the neuronal lineage markers DCX (red) and NeuN (green) at DIV 3, 7 and 10 post-seeding in the different conditions. **(B)** Quantification of the proportion of DCX+, **(C)** NeuN+ and (D) DCX+/NeuN+ double stained positive cells. *$p<0.05$ compared to laminin. ***$p<0.001$ between the treatments NanoPDA and NanoGO, Holm-Sidak method One Way Analysis of Variance on Ranks. Scale bar, 50 µm.

Journal Pre-proof

Figures

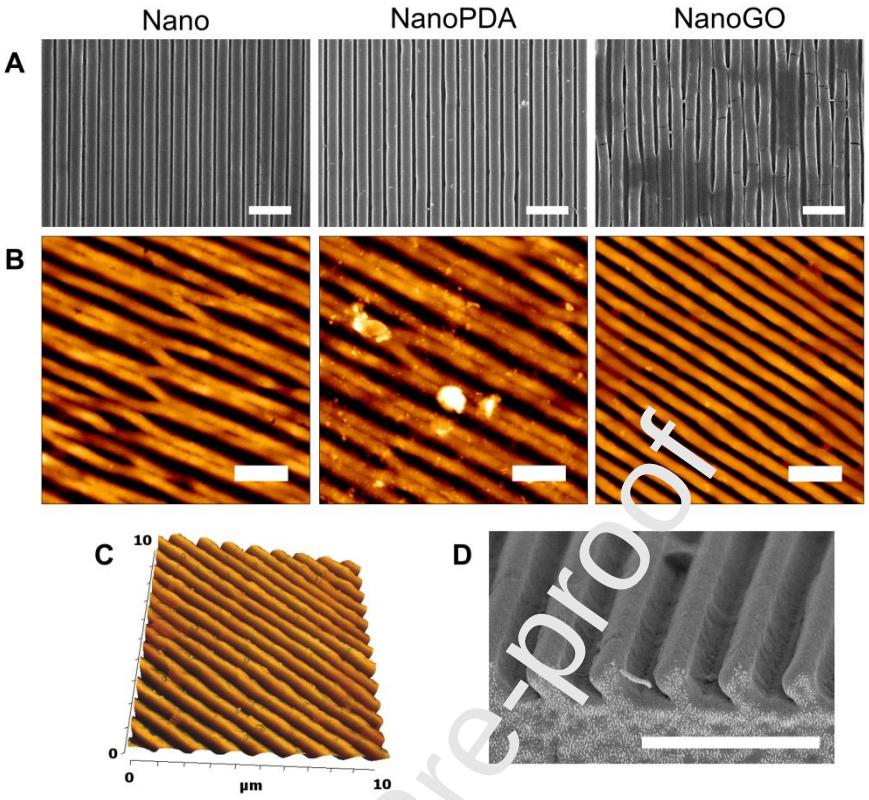

Figure 1

Journal Pre-proof

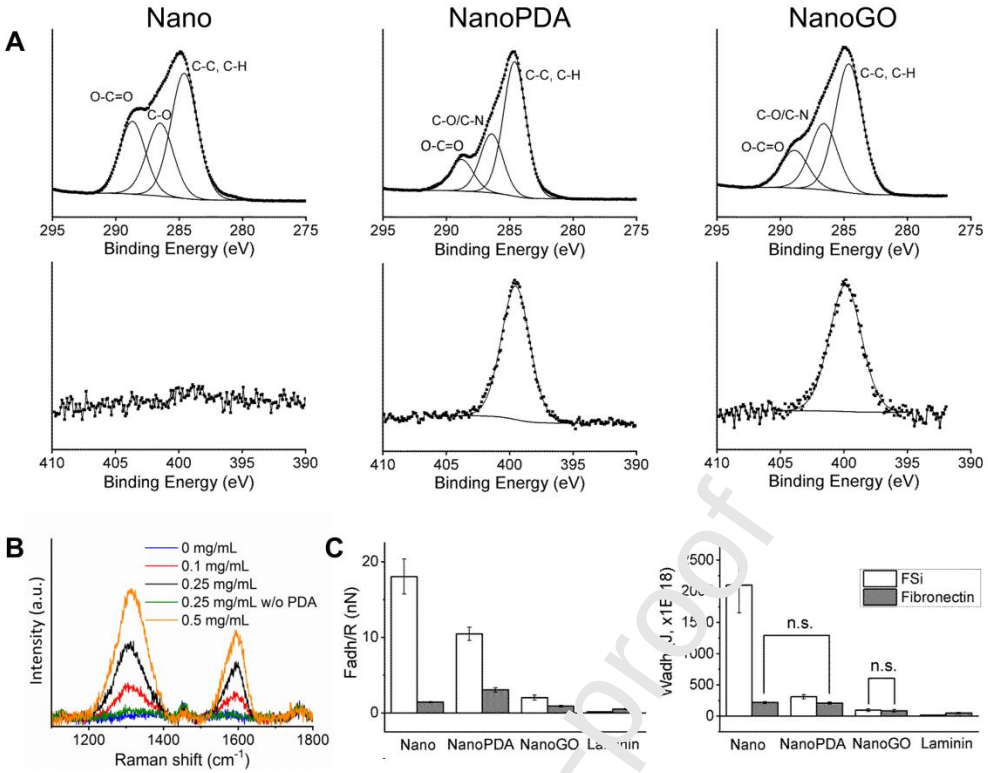

Figure 2

Journal Pre-proof

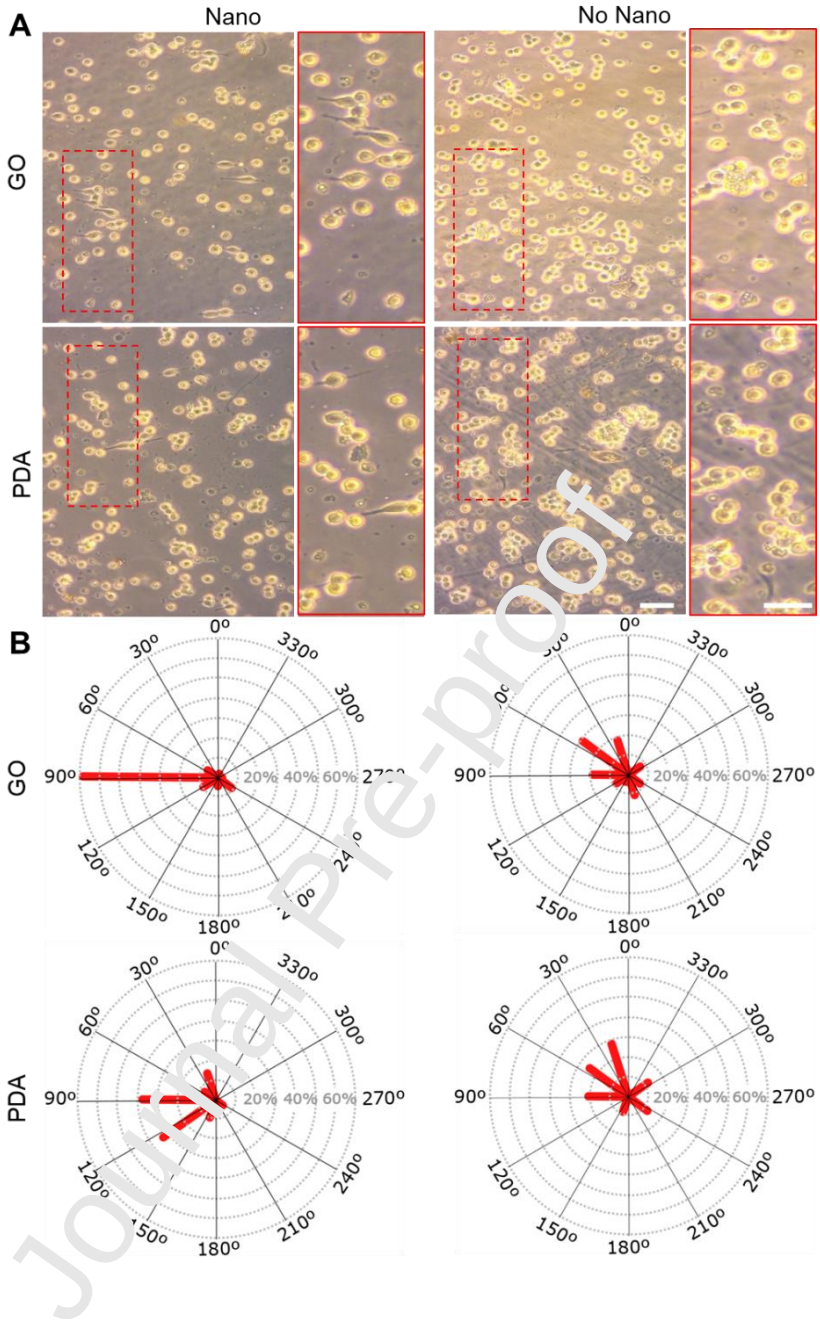

Figure 3

Journal Pre-proof

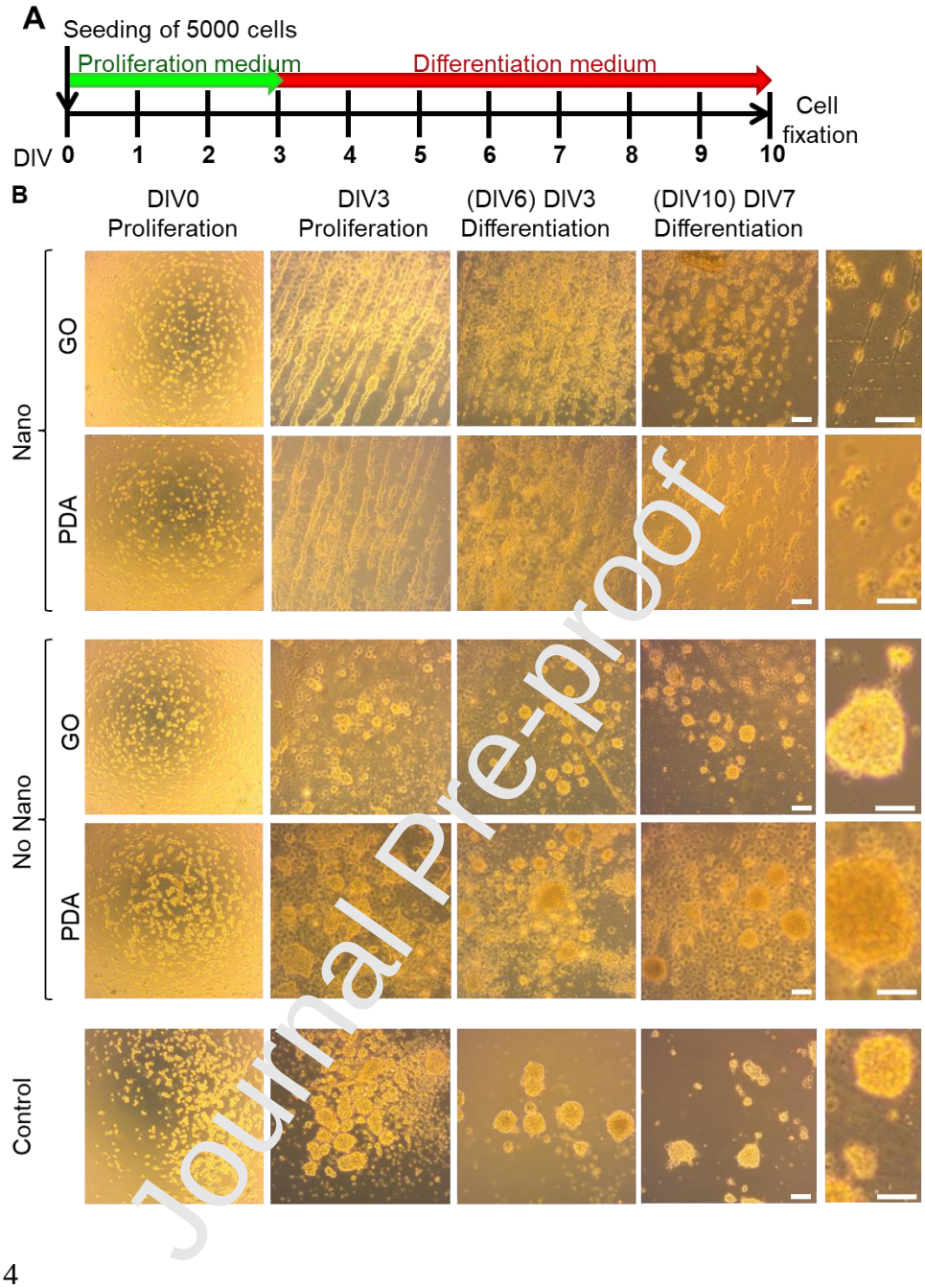

Journal Pre-proof

Figure 4

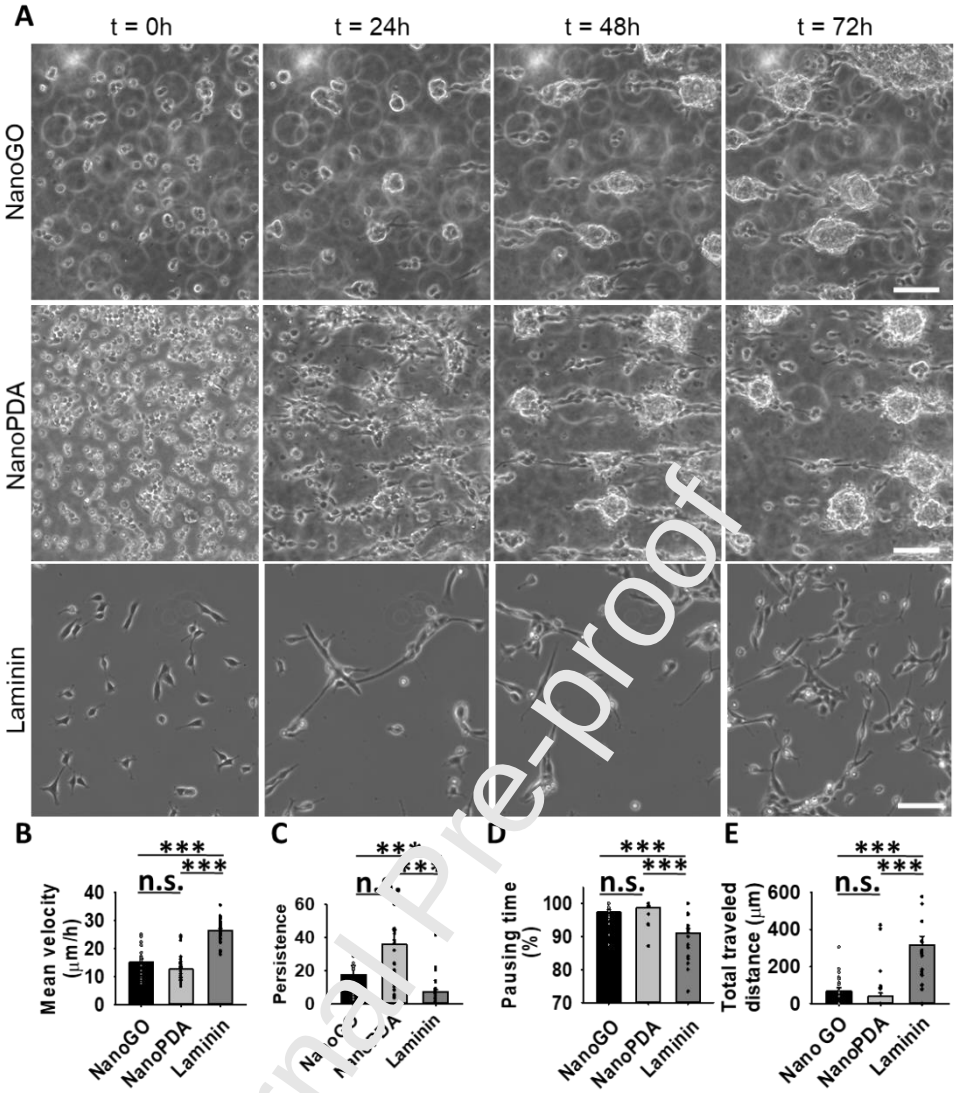

Figure 5

Journal Pre-proof

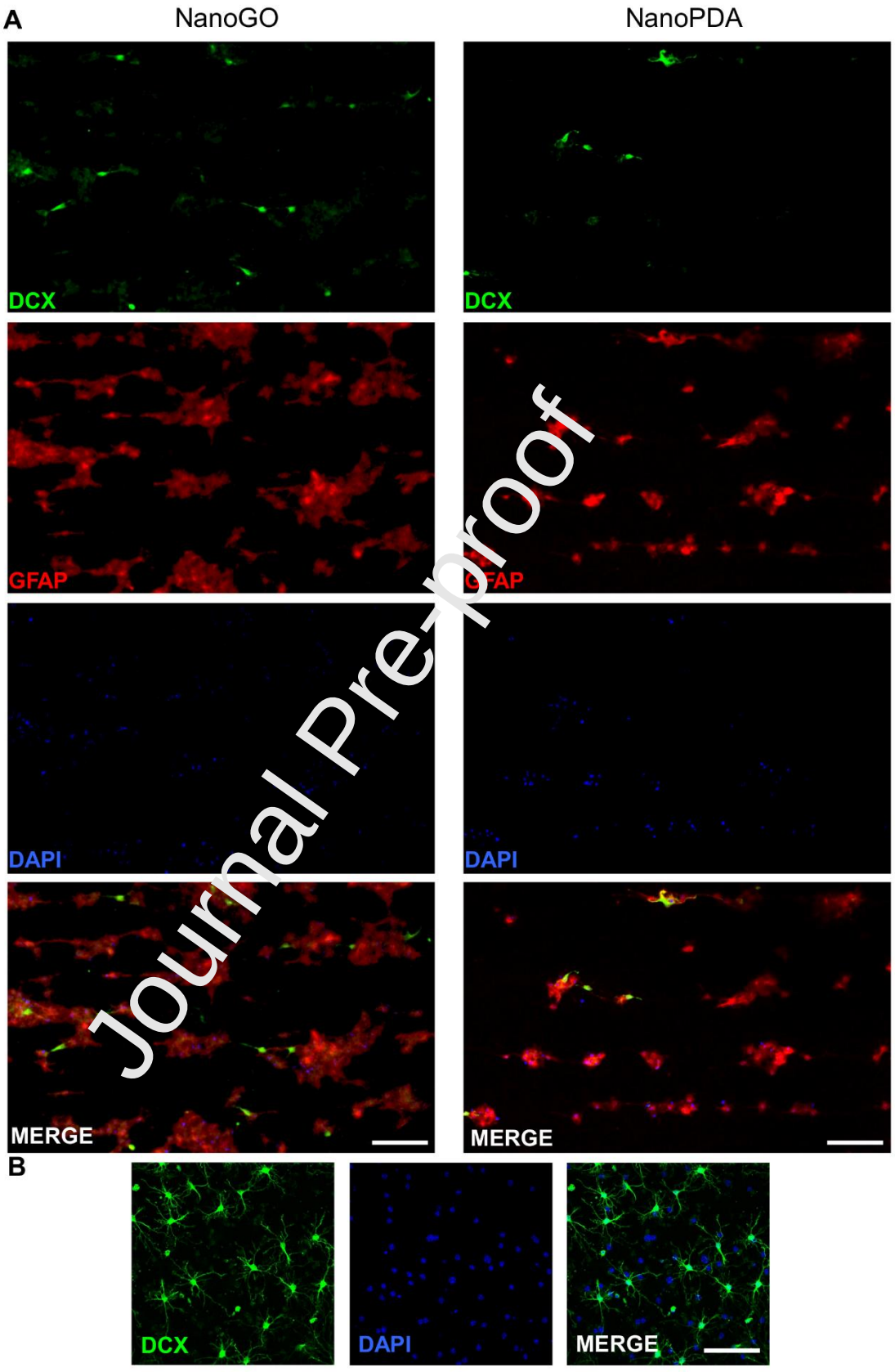

Journal Pre-proof

Figure 6

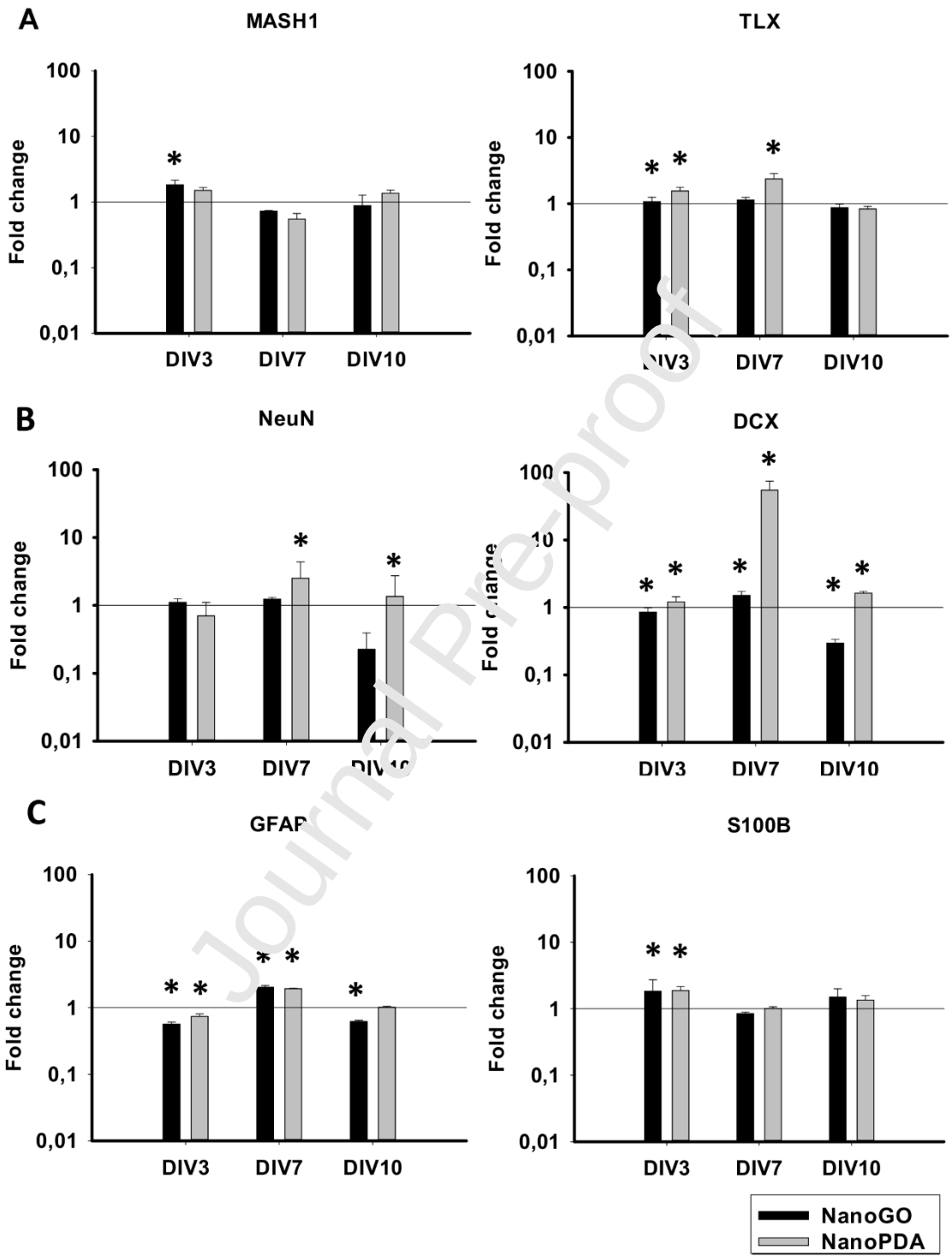
A
MASH1
TLX
B
NeuN
DCX
C
GFAP
S100B
Fold change
100
10
1
0,1
0,01
DIV3
DIV7
DIV10
NanoGO
NanoPDA

Figure 7

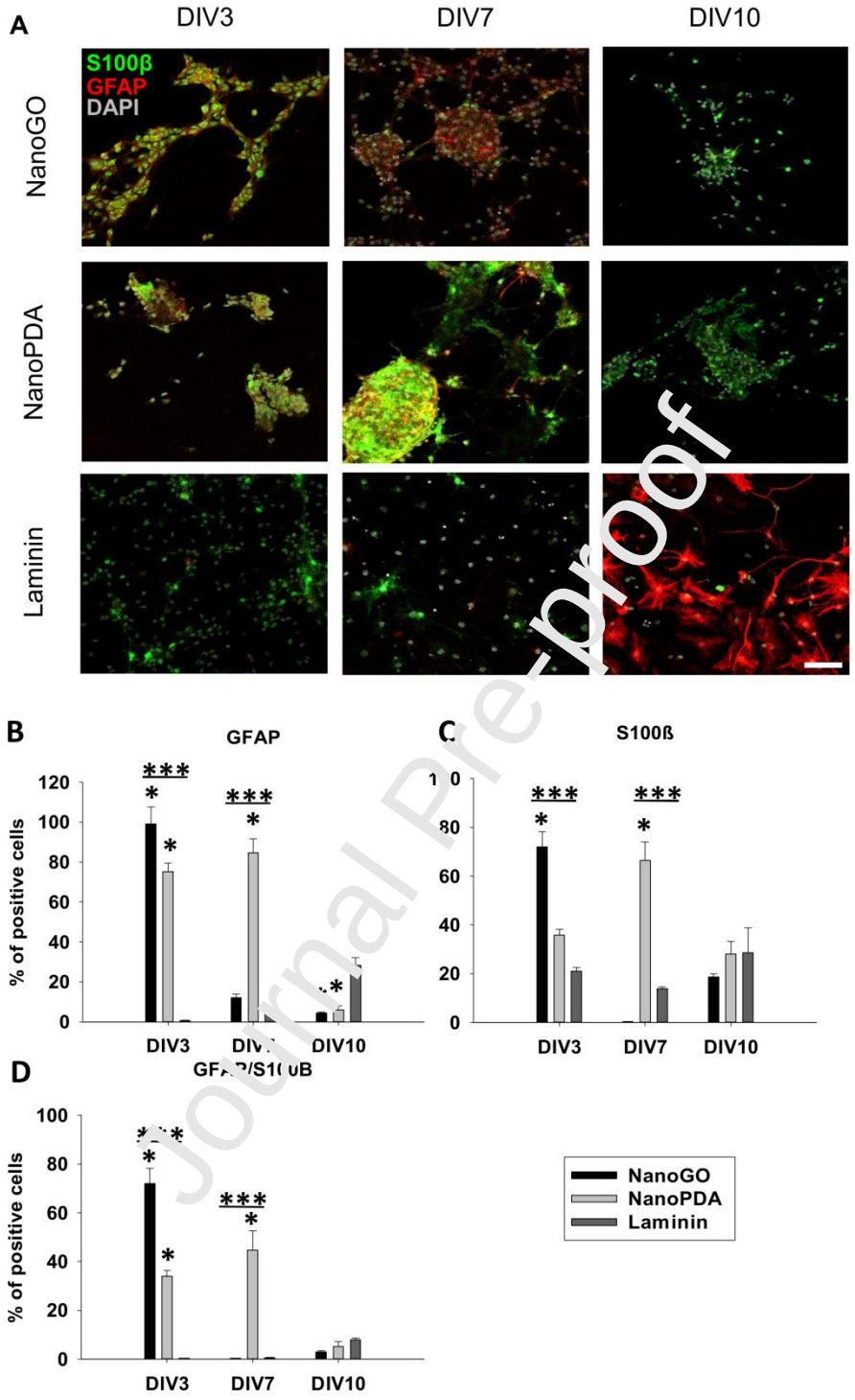

Figure 8

Journal Pre-proof

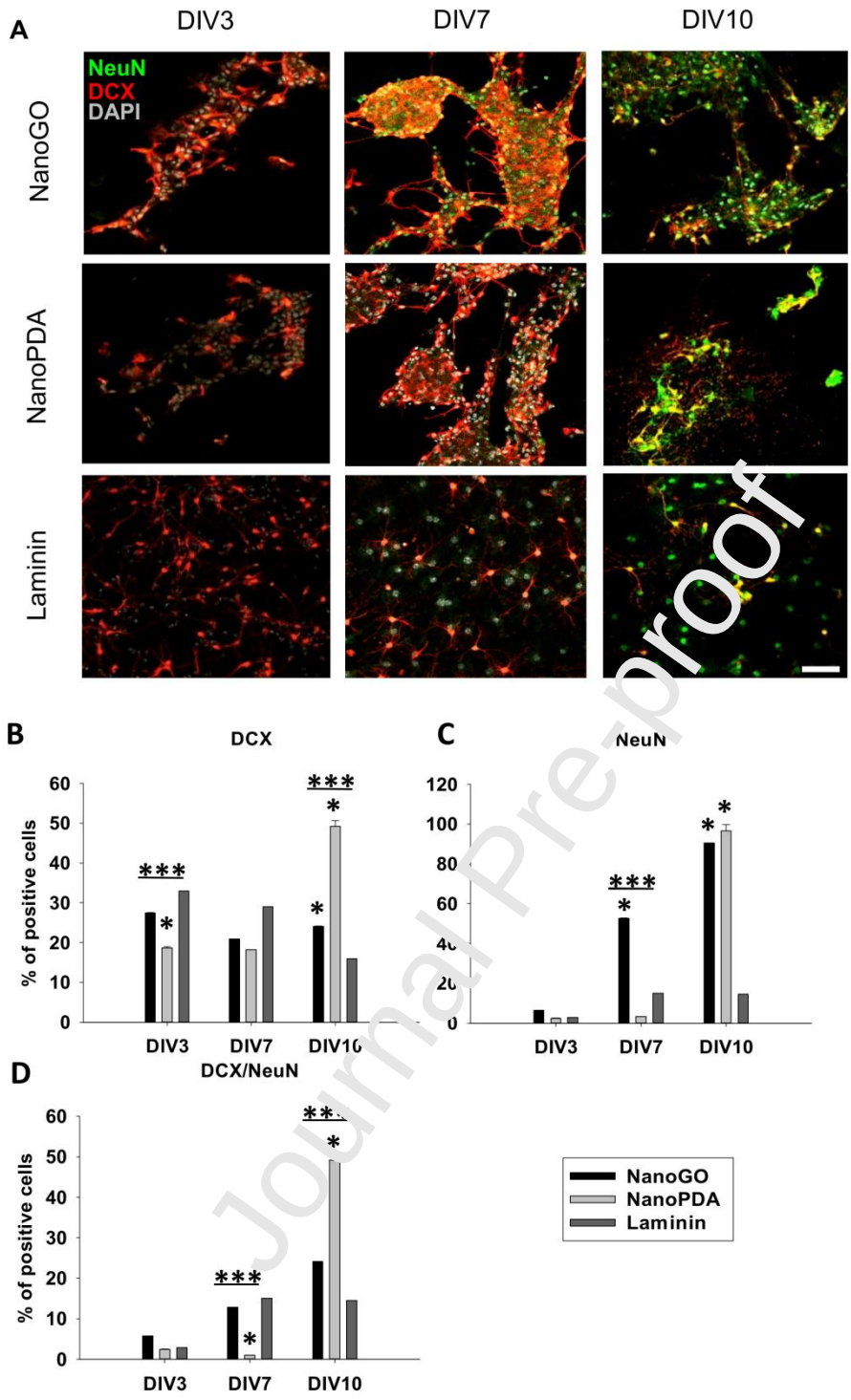

Figure 9

Journal Pre-proof

Graphical Abstract

In the present work we describe the fabrication and characterization of a biodegradable nanostructured poly(L-lactide-co-ε-caprolactone) (PLCL) scaffolds either with or without graphene oxide (GO) functionalization, to support the alignment, growth, migration and differentiation of neural stem and progenitor cells without a need of a laminin coating. Furthermore, our scaffolds induce a fast and efficient cell differentiation towards neuronal lineages while maintaining a glial cell population, which makes these materials a very attractive neural repair compounds for future therapeutic approaches.

Journal Pre-proof

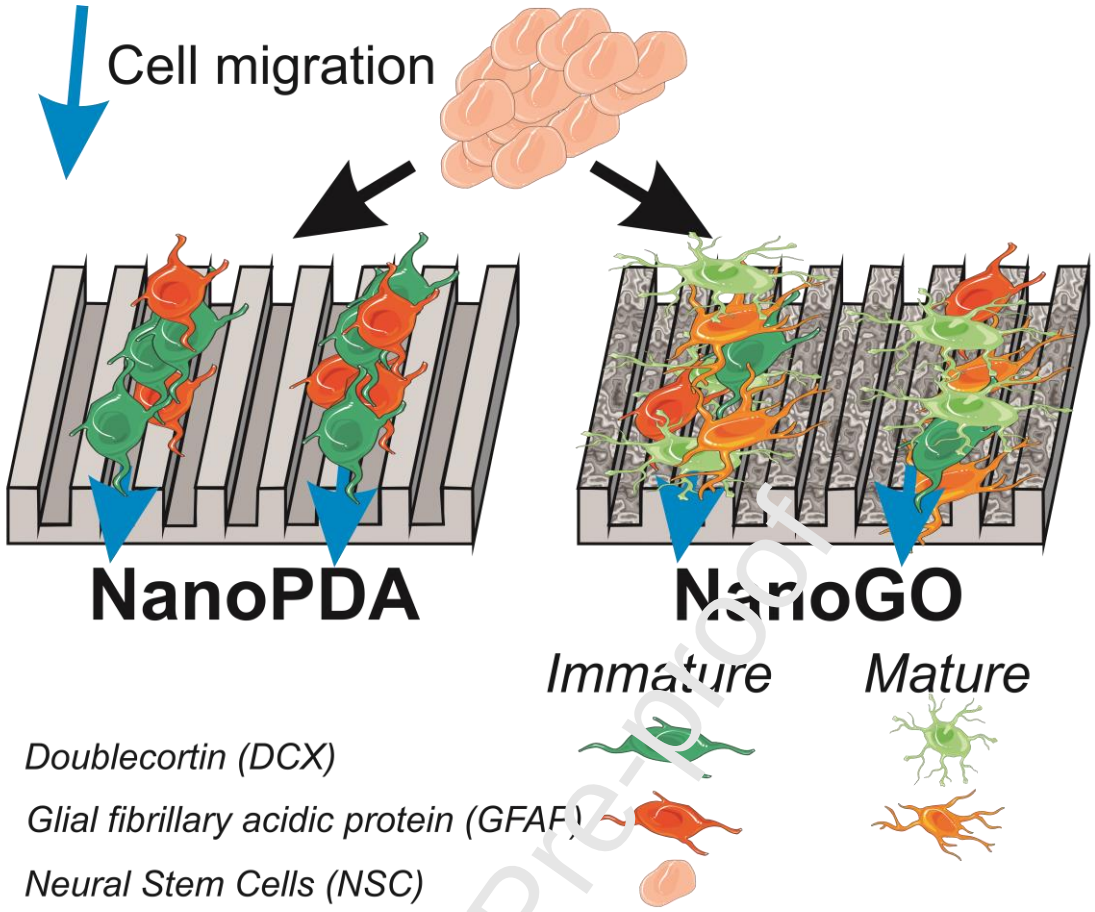

Journal Pre-proof

Highlights

- Thermoplastic nanopatterning of FDA-approved elastomeric bioresorbable polymer.
- Polydopamine-mediated surface functionalization with graphene oxide.
- Migration paths for neural stem and progenitor cells are created.
- Fast and efficient stem cell differentiation towards neuronal lineages.

Journal Pre-proof

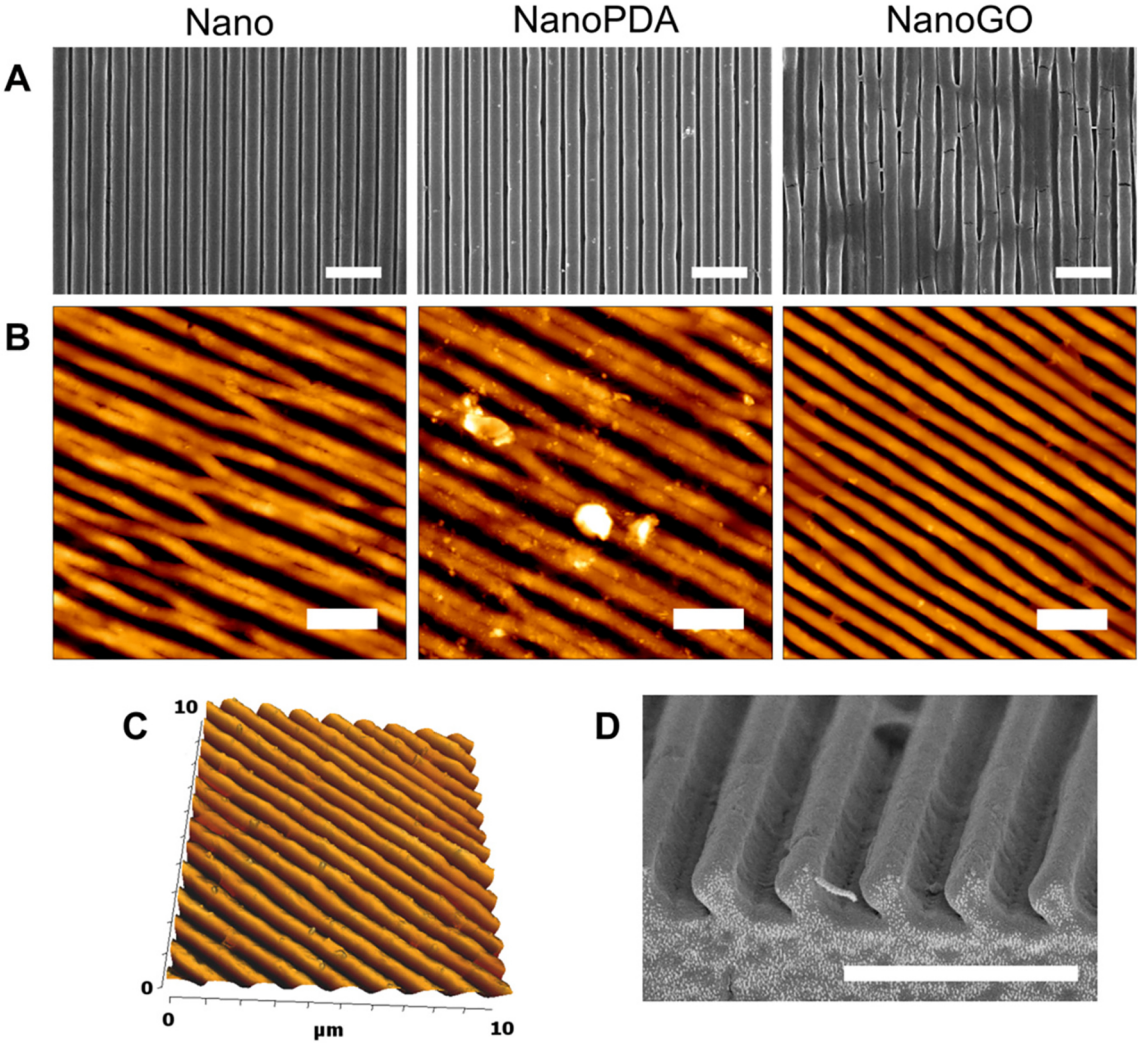

Figure 1

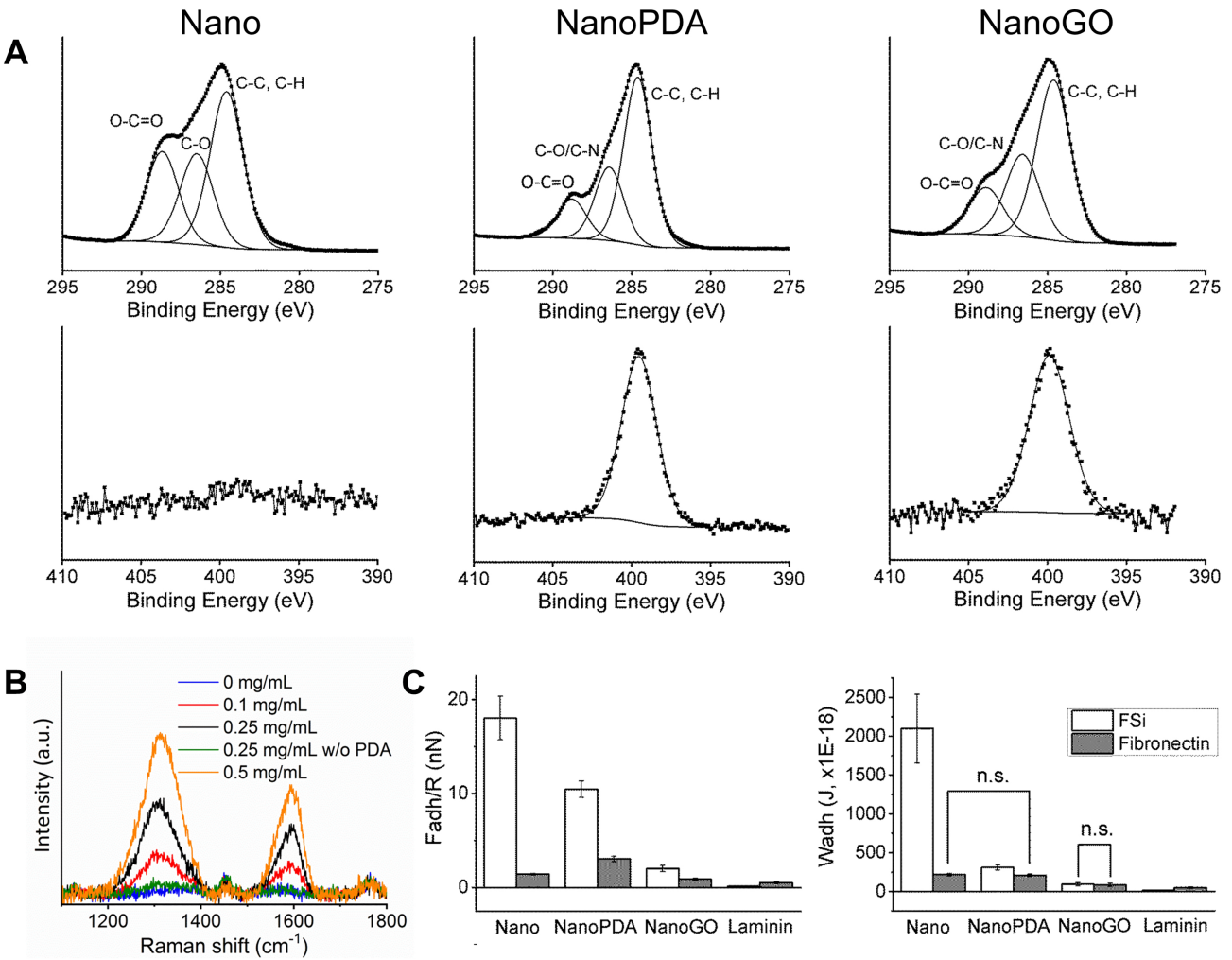
A
Nano
NanoPDA
NanoGO
O-C=O
C-O
C-C, C-H
C-O/C-N
Binding Energy (eV)
B
0 mg/mL
0.1 mg/mL
0.25 mg/mL
0.25 mg/mL w/o PDA
0.5 mg/mL
Intensity (a.u.)
Raman shift (cm-1)
C
Fadh/R (nN)
Wadh (J, x1E-18)
FSi
Fibronectin
n.s.
Nano
NanoPDA
NanoGO
Laminin

Figure 2

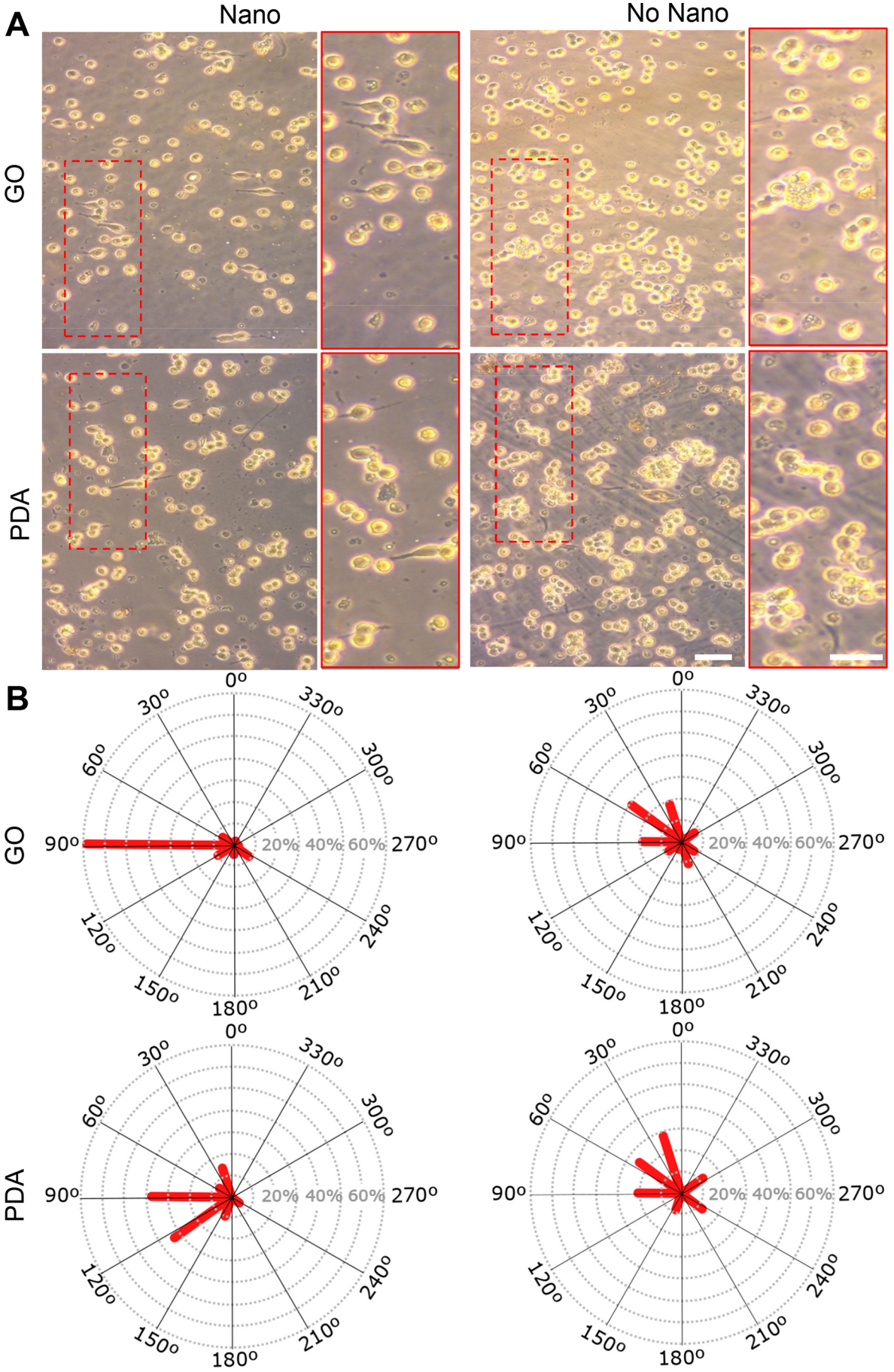
A
Nano
No Nano
GO
PDA
B
GO
PDA
0°
30°
60°
90°
120°
150°
180°
210°
240°
270°
300°
330°
20%
40%
60%

Figure 3

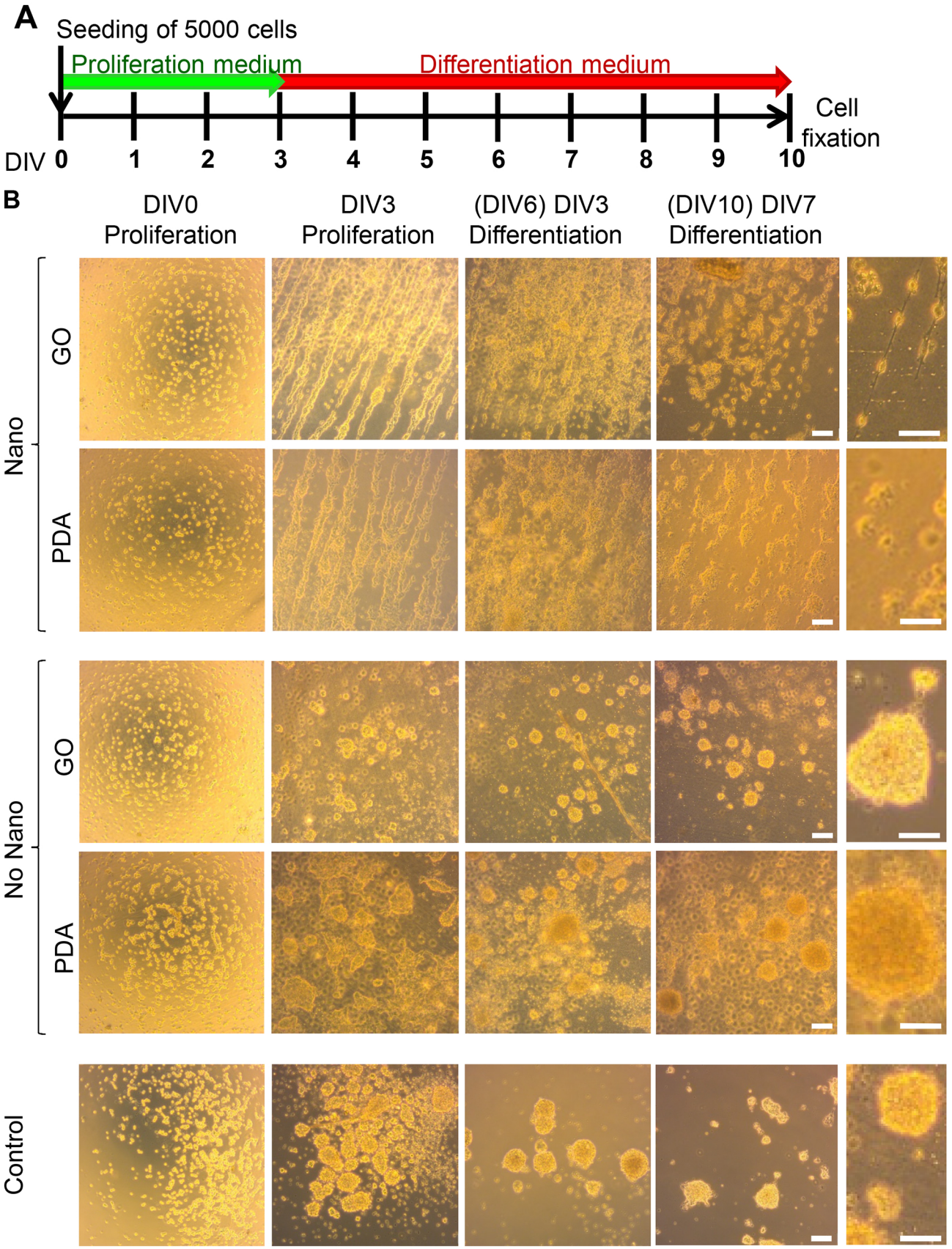
A
Seeding of 5000 cells
Proliferation medium
Differentiation medium
Cell fixation
DIV 0 1 2 3 4 5 6 7 8 9 10
B
DIV0 Proliferation
DIV3 Proliferation
(DIV6) DIV3 Differentiation
(DIV10) DIV7 Differentiation
Nano
GO
PDA
No Nano
GO
PDA
Control

Figure 4

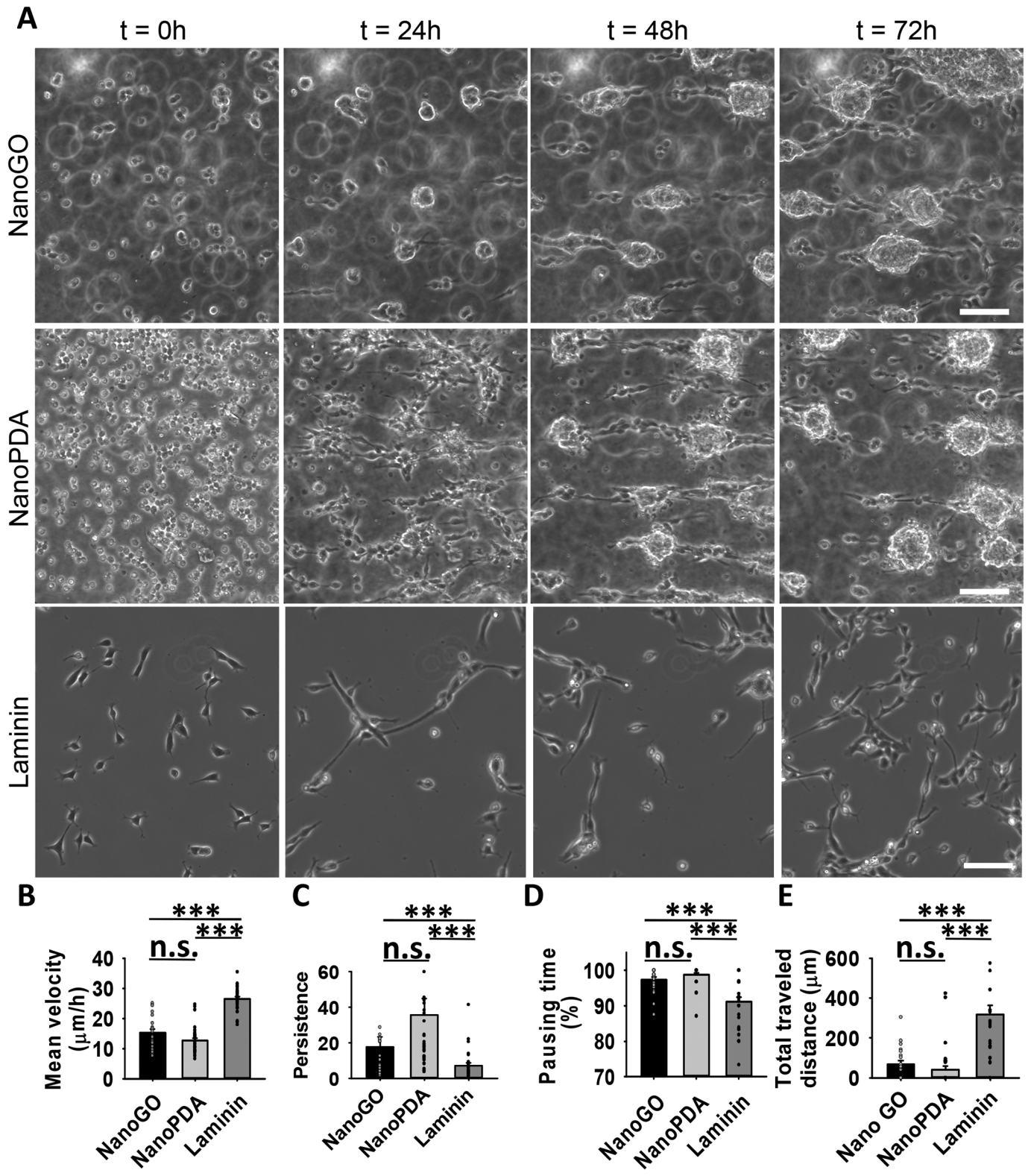
A
t = 0h
t = 24h
t = 48h
t = 72h
NanoGO
NanoPDA
Laminin
B
Mean velocity (μm/h)
C
Persistence
D
Pausing time (%)
E
Total traveled distance (μm)
n.s.
***
NanoGO
NanoPDA
Laminin
Nano GO

Figure 5

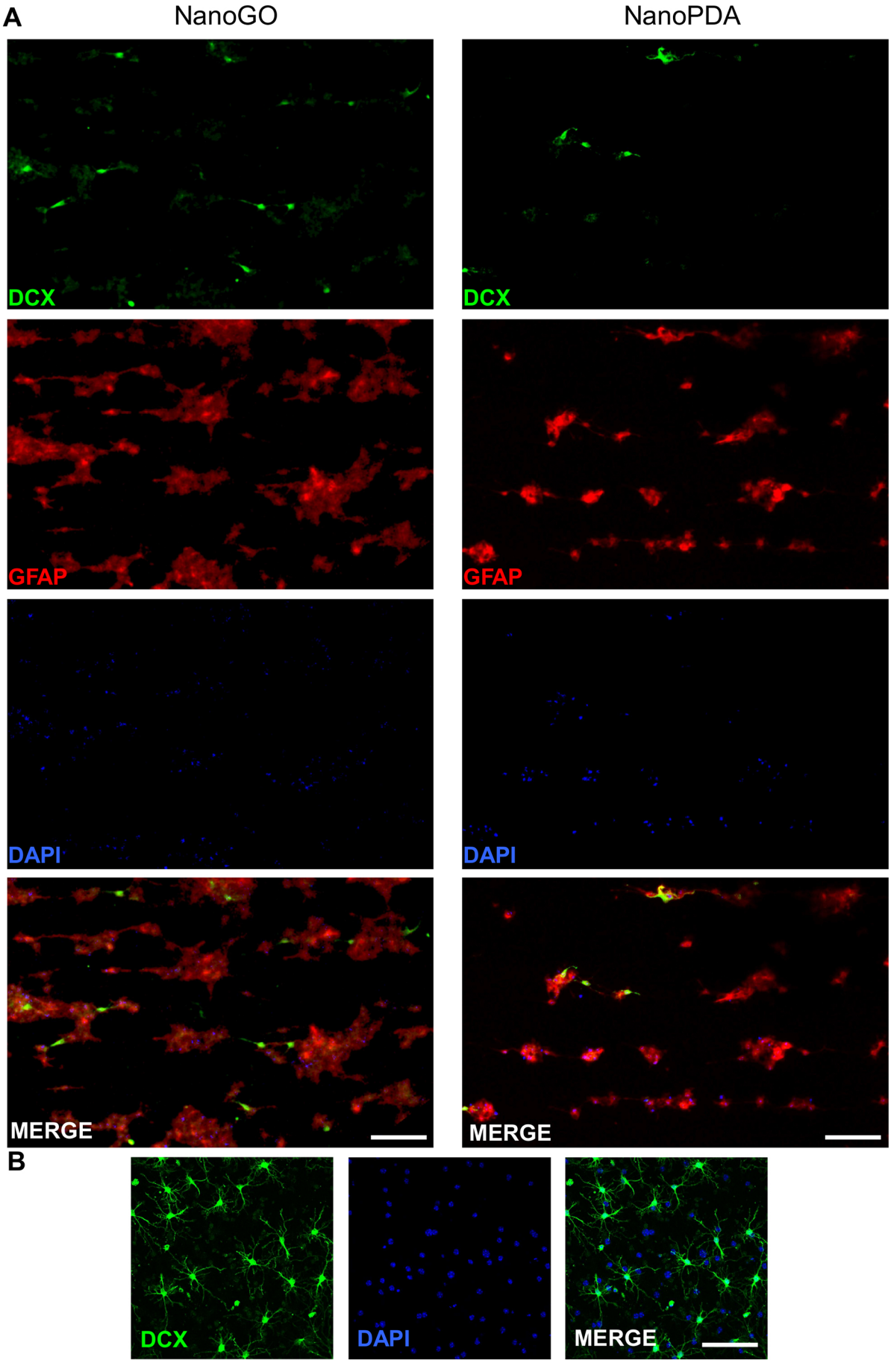
A
NanoGO
NanoPDA
DCX
DCX
GFAP
GFAP
DAPI
DAPI
MERGE
MERGE
B
DCX
DAPI
MERGE

Figure 6

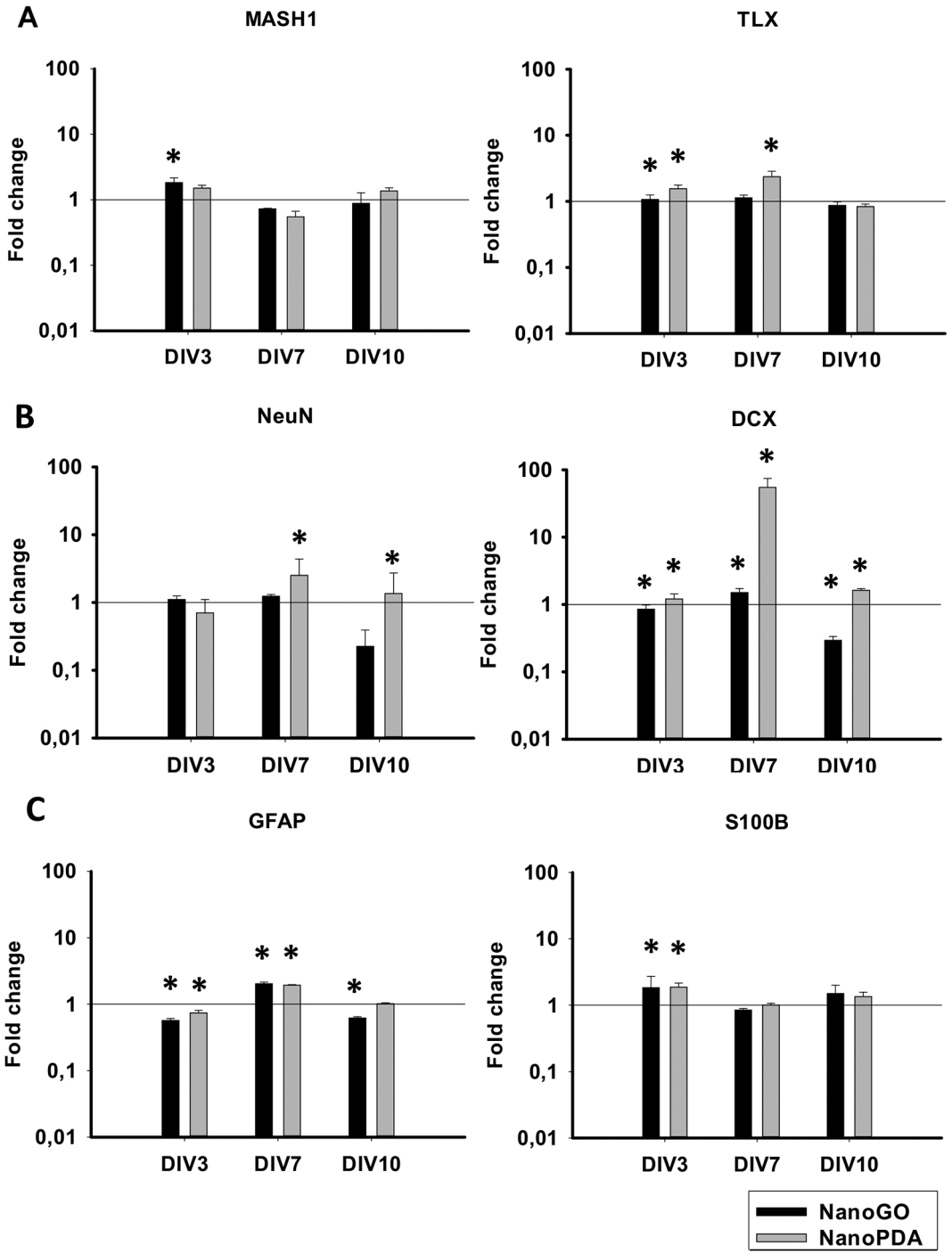
A
MASH1
TLX
B
NeuN
DCX
C
GFAP
S100B
Fold change
100
10
1
0,1
0,01
DIV3
DIV7
DIV10
NanoGO
NanoPDA

Figure 7

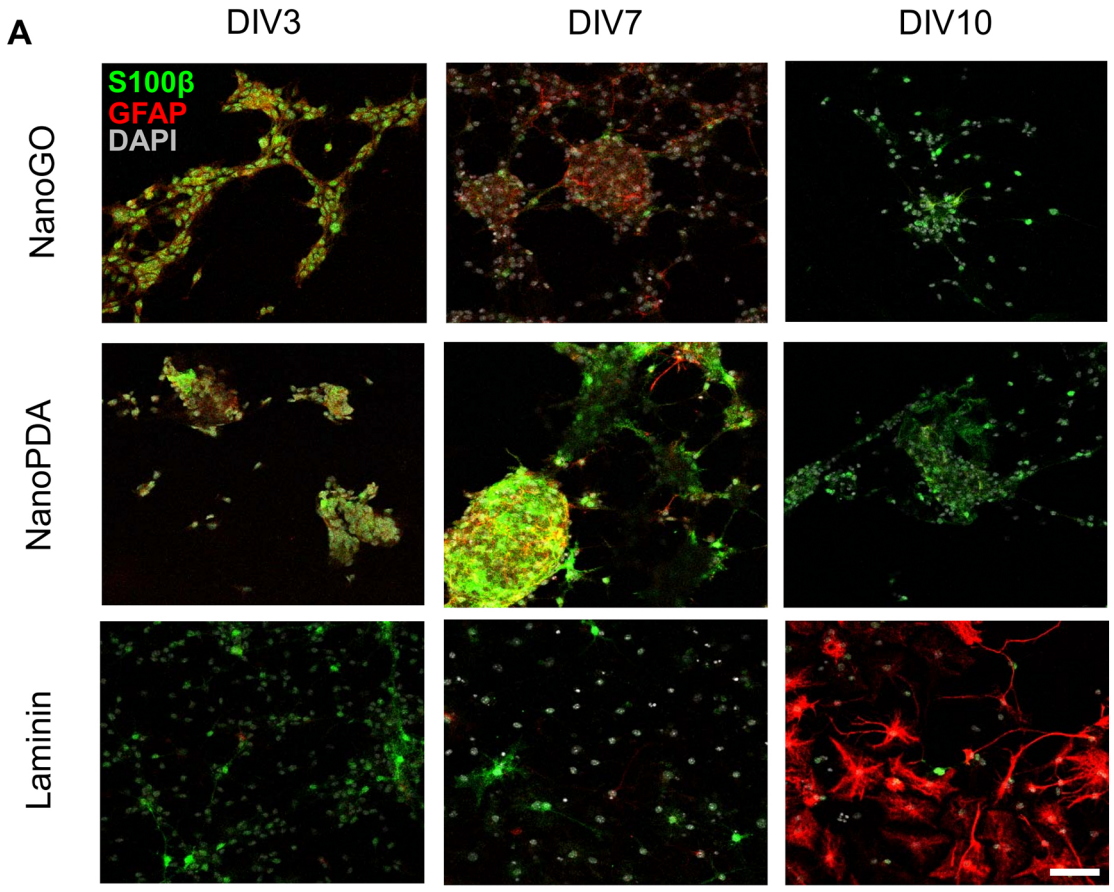
A
DIV3
DIV7
DIV10
S100β
GFAP
DAPI
NanoGO
NanoPDA
Laminin

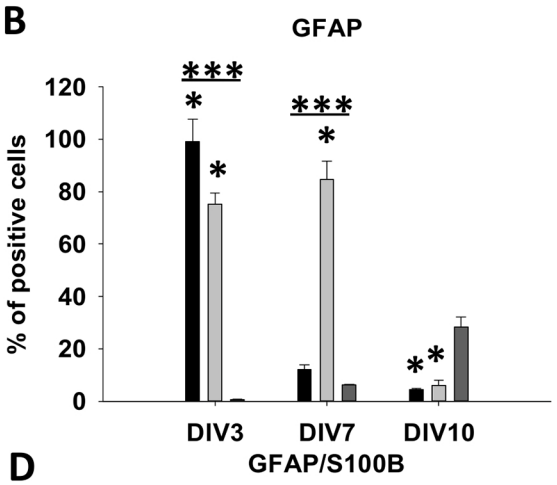
B
GFAP
% of positive cells
120
100
80
60
40
20
0
***
*
*
***
*
**
DIV3
DIV7
DIV10

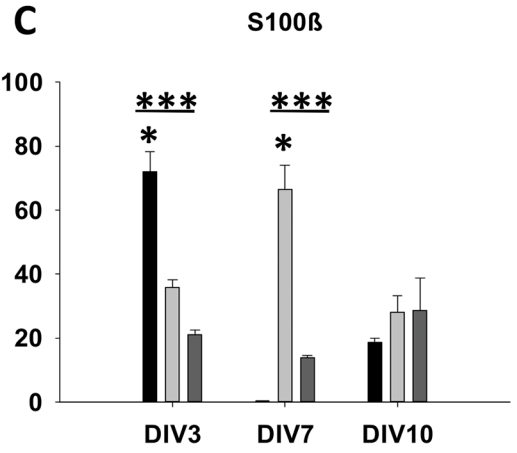
C
S100ß
100
80
60
40
20
0
***
*
***
*
DIV3
DIV7
DIV10

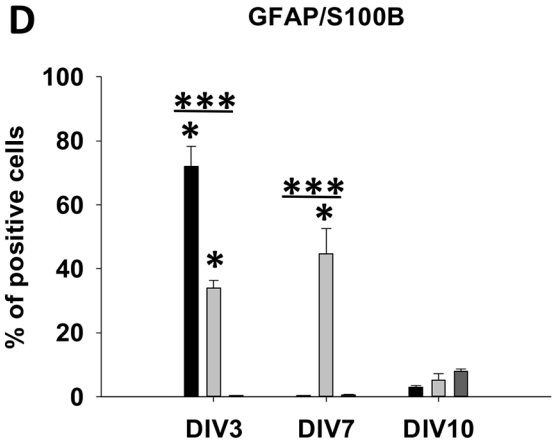
D
GFAP/S100B
% of positive cells
100
80
60
40
20
0
***
*
*
***
*
DIV3
DIV7
DIV10

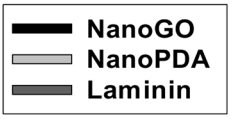
NanoGO
NanoPDA
Laminin

Figure 8

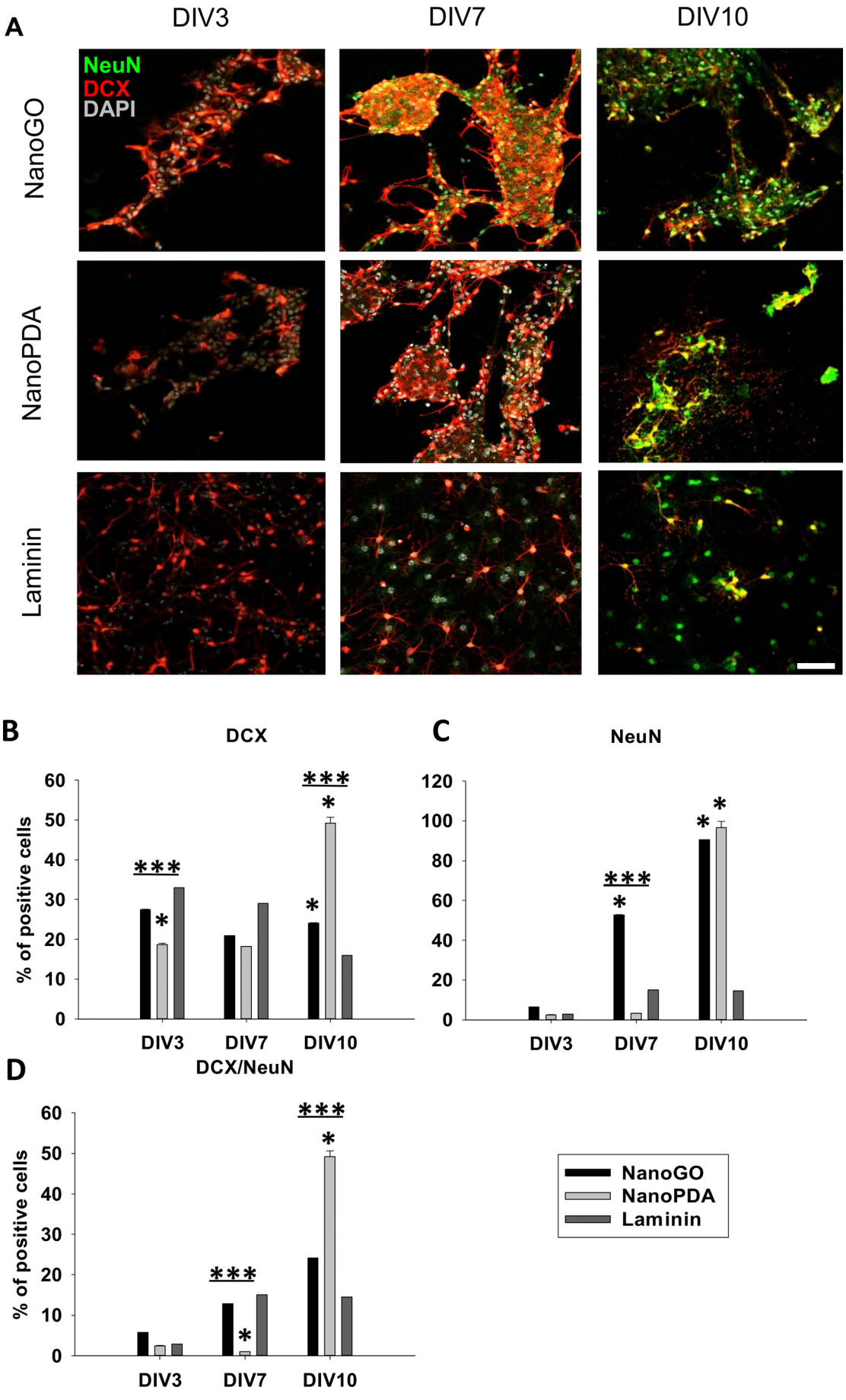
A
DIV3
DIV7
DIV10
NeuN
DCX
DAPI
NanoGO
NanoPDA
Laminin
B
DCX
% of positive cells
DIV3
DIV7
DIV10
DCX/NeuN
C
NeuN
D
NanoGO
NanoPDA
Laminin

Figure 9